Z_2 Non-Restoration and Composite Higgs:
Singlet-Assisted Baryogenesis w/o Topological Defects

Andrei Angelescu, Florian Goertz, and Aika Tada

Max-Planck-Institut für Kernphysik
Saupfercheckweg 1, 69117 Heidelberg, Germany
E-mail: andrei.angelescu@mpi-hd.mpg.de,
florian.goertz@mpi-hd.mpg.de, aika.tada@mpi-hd.mpg.de

ABSTRACT: Simple scalar-singlet extensions of the Standard Model with a (spontaneously broken) Z_2 symmetry allow for a strong first order electroweak phase transition, as sought in order to realize electroweak baryogenesis. However they generically also lead to the emergence of phenomenologically problematic domain walls. Here we present a framework with a real scalar singlet that features a different thermal history that avoids this problem by never restoring the Z_2 symmetry in the early universe. This is accomplished by considering $D > 4$ operators that emerge on general grounds, understanding the model as the low energy tail of a more complete theory, like for example in composite Higgs scenarios. Sticking to the latter framework, we present a concrete $SO(6)/SO(5)$ composite realization of the idea. To this end, we additionally provide a complete classification of the structure of the Higgs potential (and the Yukawa couplings) in $SO(6)/SO(5)$ models with fermions in the $\mathbf{1}, \mathbf{6}, \mathbf{15}$ or $\mathbf{20'}$ of $SO(6)$.

Contents

1   Introduction

Understanding how a baryon-asymmetric universe, as we observe it, could have emerged is one of the most important issues in particle physics and cosmology. In fact, this seems to require an extension of the Standard Model (SM) of Particle Physics, which fails to fulfill (quantitatively) two of the three Sakharov criteria [1] for generating the baryon asymmetry, namely a deviation from thermal equilibrium and the presence of substantial CP violation.

Extensions of the SM with a scalar singlet η are promising candidates for baryogenesis at the electroweak scale, by inducing a strong first order electroweak phase transition (EWPhT), providing the out-of-equilibrium situation, and allowing for additional sources of CP violation. A particularly well studied class of models envisages a real scalar with a $Z_2 : \eta \to -\eta$ symmetry (similar to what emerges in non-minimal composite Higgs models [2, 3]) – which makes η contribute to the dark matter abundance, while being protected from collider constraints. Such setups have been shown to allow for a sufficiently strong EWPhT to preserve an adequate baryon asymmetry [3–13].

A generic challenge in this setting is however the appearance of topological defects, associated to the spontaneous breaking of the Z_2 symmetry after η acquires a vacuum expectation value (vev) $|\langle\eta\rangle| \equiv v_\eta$ in the thermal evolution of the universe.

Patches with $\langle \eta \rangle = +v_\eta$ and $\langle \eta \rangle = -v_\eta$ would get equally populated, which would on the one hand produce potentially dangerous domain walls at the boundaries [14], and on the other lead to a cancellation between produced baryon and antibaryon excesses (see, e.g., [3]), requiring additional model building.

Here we show how a minimal change in the scalar potential can solve these issues via a thermal history in which the Z_2 was never a symmetry of the ground state.[1] In fact, adding higher powers of the scalar-singlet field to the potential can allow for Z_2 symmetry non-restoration (SNR) at high temperatures, as we will show below. Such higher dimensional operators are expected to be generated in the presence of new physics addressing other problems of the SM, such as the hierarchy problem or the flavor puzzle.

After having studied the idea in this effective field theory (EFT) extension of the SM in Section 2, in Section 3 we will provide an explicit realization in the form of a composite Higgs (CH) scenario with $SO(6)/SO(5)$ breaking pattern [2], where we will unveil parameter space that had not been considered before. More generally, we will present a comprehensive survey of the Higgs potential in such next-to-minimal CH models (nMCHMs) for various fermion embeddings and explore their peculiarities, both in general and with respect to the question of generating the sought form of the potential for Z_2 SNR. In Section 4 we will then match the most promising CH setup to the IR EFT and explore the CH parameter space that leads to a viable SNR. We conclude in Section 5 and provide the Yukawa couplings emerging in the various combinations of $SO(6)$ representations in Appendix A for completeness.

2 Z_2 Non-Restoration at High Temperature in Singlet EFT

In the following, we outline a simple Higgs + singlet scenario which exhibits Z_2 SNR at high temperature. While present at $T = 0$, the Z_2 symmetry under which the singlet is odd starts out as broken at high T, so as to avoid the formation of topological defects associated with the spontaneous breaking of a discrete symmetry. Therefore, in our envisaged thermal history, the Universe undergoes only one phase transition, which breaks electroweak (EW) symmetry and restores the Z_2 symmetry. If strongly first–order (SFO), this EWPhT can fulfill Sakharov's third condition, leading to EW baryogenesis (EWBG), provided there is enough CP violation.

As shown later on, with the given particle content such a scenario cannot be realized at the renormalizable level. However, it can be minimally achieved by extending the renormalizable potential with a dimension–6 singlet–only sextic term.[2]

---

[1]An alternative approach would be to add a small amount of *explicit* Z_2 breaking [3, 15].

[2]We note that higher-dimensional operators have beend studied extensively in scalar-singlet extensions, however not in the context of the phase transition but rather for injecting additional CP violation [9, 16]. Once lifted to an EFT, there is then no reason to not consider other $D = 6$ operators (which also appear generically in CH realizations [2, 3]), as done here.

Denoting by h (η) the background value of the Higgs (singlet) scalar, the $T = 0$ tree level potential reads:

$$V_{\text{tree}}(h, \eta) = \frac{\mu_h^2}{2} h^2 + \frac{\lambda_h}{4} h^4 + \frac{\mu_\eta^2}{2} \eta^2 + \frac{\lambda_\eta}{4} \eta^4 + \frac{\lambda_{h\eta}}{2} h^2 \eta^2 + \frac{\eta^6}{\Lambda^2}. \qquad (2.1)$$

For the temperature–dependent part of the potential, we work in the high–temperature expansion and retain only the leading T^2 contributions:

$$V_T(h, \eta, T) = \frac{T^2}{2} (c_h h^2 + c_\eta \eta^2) + \frac{5T^2}{4\Lambda^2} \eta^4, \qquad (2.2)$$

which are added to Eq. (2.1) to obtain the full potential, denoted as

$$V(h, \eta, T) \equiv V_{\text{tree}}(h, \eta) + V_T(h, \eta, T). \qquad (2.3)$$

Taking into account the leading corrections coming from the top quark and the gauge and scalar sectors, the $c_{h,\eta}$ coefficients are given by:

$$c_h = \frac{1}{48} \left(9g_2^2 + 3g_1^2 + 12y_t^2 + 24\lambda_h + 4\lambda_{h\eta} \right), \quad c_\eta = \frac{\lambda_{h\eta}}{3} + \frac{\lambda_\eta}{4}. \qquad (2.4)$$

With or without the dimension–6 η^6 term, the necessary and sufficient condition for Z_2 SNR at high temperatures is to have a negative c_η. This way, for sufficiently high T, the coefficient of the η^2 term becomes negative, i.e. $\mu_\eta^2 + c_\eta T^2 < 0$, which destabilizes the origin and sets the global minimum of the potential at $(h, \eta) = (0, w)$.

In the renormalizable case, corresponding to $\Lambda \to \infty$, one needs $\lambda_\eta > 0$ in order to avoid a runaway direction in the potential, which means that Z_2 SNR requires $\lambda_{h\eta} < 0$, cf. Eq. (2.4). At the same time, in order to achieve the desired thermal history of the Universe, we require the coexistence (at intermediate temperatures) of two minima, the Z_2–breaking $(0, w)$ and EW minimum $(v, 0)$, which become degenerate at the critical temperature T_c. The existence of the $(0, w)$ minimum at $T = T_c$ implies that the second derivative of the potential along the h direction is positive at $h = 0$, i.e.

$$V_{hh}(0, w(T_c), T_c) = \mu_h^2 + c_h T_c^2 + \lambda_{h\eta} w(T_c)^2 > 0. \qquad (2.5)$$

Furthermore, since the potential contains only h^2 and h^4 terms, the existence of the EW minimum at $T = T_c$ implies that the origin is unstable along the h direction, namely

$$V_{hh}(0, 0, T_c) = \mu_h^2 + c_h T_c^2 < 0. \qquad (2.6)$$

From the two conditions from Eqs. (2.5) and (2.6), it follows that $\lambda_{h\eta} > 0$, which is in contradiction with the SNR condition $\lambda_{h\eta} < 0$. Therefore, as pointed out previously, Z_2 SNR cannot be achieved at the renormalizable level in the Higgs + Z_2–odd singlet scenario.

Including the S^6 term, the conditions from Eqs. (2.5) and (2.6) still have to be fulfilled, which means the requirement $\lambda_{h\eta} > 0$ remains. Now, the only way of

obtaining $c_\eta < 0$ is to have a negative λ_η (as we assume from here on), which becomes viable due to the introduction of the η^6 term. The role of the latter is to ensure that the potential remains bounded from below along the η direction, and it turns out to be sufficient for accommodating Z_2 SNR. This is the motivation behind considering the $T = 0$ potential from Eq. (2.1).

Before performing a numerical analysis of the thermal history induced by the full potential in Eq. (2.3), we present its main analytical features, namely its (T–dependent) critical points. The one at the origin, i.e. at $(h, \eta) = (0,0)$, starts as a saddle point at high–T, and later on can turn into a (local) maximum or remain a saddle point. The EW minimum at $(v, 0)$ develops as soon as

$$v^2(T) = -\frac{\mu_h^2 + c_h T^2}{\lambda_h} \tag{2.7}$$

becomes positive, leading to a real $v(T)$. Along the η direction, the presence of the η^6 terms leads to the existence of two critical points at $(0, w_\pm)$, with

$$w_\pm^2(T) = \frac{\Lambda^2}{12} \left(-\lambda_\eta - 5\frac{T^2}{\Lambda^2} \pm \sqrt{\lambda_\eta^2 - 24\frac{\mu_\eta^2}{\Lambda^2} + 4\frac{T^2}{\Lambda^2}(\lambda_\eta - 2\lambda_{h\eta}) + 25\frac{T^4}{\Lambda^4}} \right). \tag{2.8}$$

The critical point at $(0, w_+)$ starts as the Z_2–breaking global minimum at high–T, and can either remain a minimum till $T = 0$ or turn into a saddle point. As long as $w_-(T)^2 > 0$, $(0, w_-)$ exists as a critical point and is either a maximum or a saddle point. Finally, there are two more possible critical points at (v_{b_-}, w_{b_-}) and (v_{b_+}, w_{b_+}), with both $v_{b_\pm} \neq 0$ and $w_{b_\pm} \neq 0$. At temperatures where it is real, the former is a saddle point and acts as a barrier between the EW and Z_2–breaking minima, rendering the EWPhT strongly first order, whereas the latter develops as a local minimum as soon as $(0, w_+)$ becomes a saddle point. Due to being rather involved, we choose not to show the analytical expressions of $v_{b_\pm}$ and $w_{b_\pm}$.

In an initial stage of our numerical analysis, we visualize the various constraints that we impose on our model. We first make sure that, at high T, the Universe starts in the Z_2–breaking minimum at $(0, w_+)$. For this, we require the origin to be destabilised at $T = \Lambda$ along the η direction:

$$V_{\eta\eta}(0, 0, T = \Lambda) = \mu_\eta^2 + c_\eta \Lambda^2 < 0, \tag{2.9}$$

which ensures that the origin is not a minimum,[3] leaving $(0, w_+)$ as the only minimum at $T = \Lambda$. We remark that here the initial condition of only populating that Z_2-breaking vacuum at high energies and not the opposite $(0, -w_+)$ could emerge

---

[3]Alternatively, one can envisage the origin as being a local miminum and $(0, w_+)$ a global minimum at high T, with a barrier separating them. However, in such a case, the Z_2–breaking minimum remains the global minimum all the way to $T = 0$, leaving EW symmetry unbroken, which is clearly an excluded scenario.
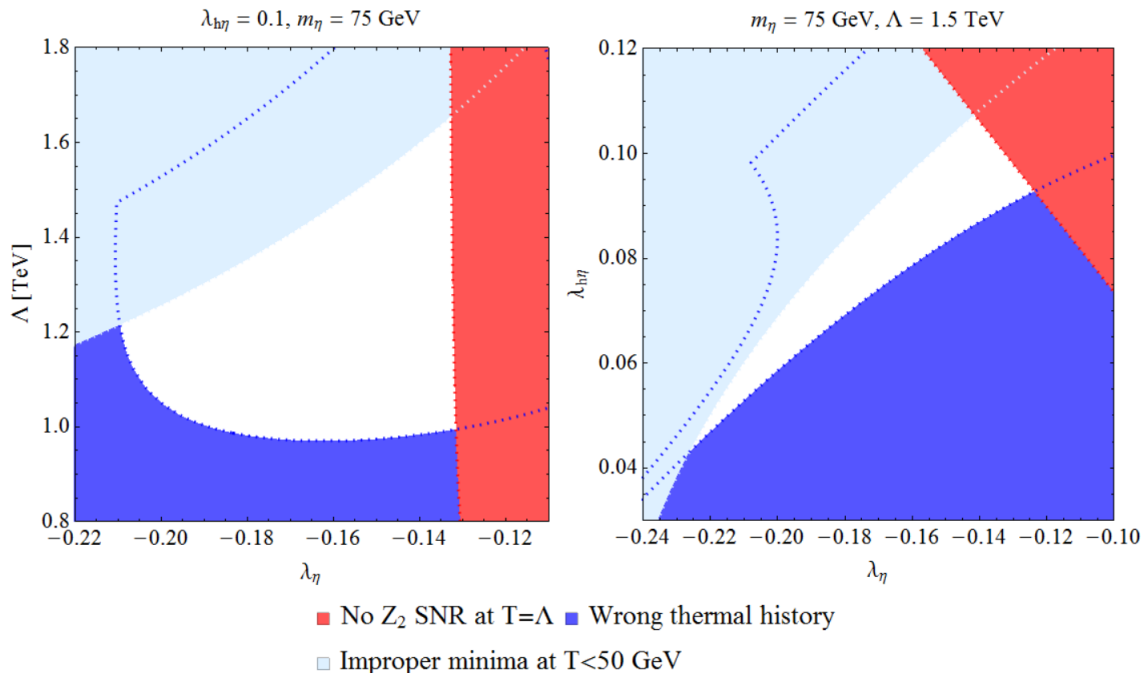
Figure 1. Visualization of the constraints that we impose in our analysis. In both panels the singlet mass has been set to $m_\eta = 75$ GeV, whereas in the left (right) panel we fix $\lambda_{h\eta} = 0.1$ ($\Lambda = 1.5$ TeV) and vary λ_η and Λ (λ_η and $\lambda_{h\eta}$). See text for the explanation of the legend.

dynamically due to inflation blowing up the corresponding patch, making it the full (visible) universe today. Other, disconnected, patches of $(0, -w_+)$ vacuum would exist, but – while the full universe would thus be baryon-symmetric – the local universe would develop an asymmetry. A more detailed and general analysis of such dynamics is left for future work. Secondly, we impose that the desired thermal history of the Universe is achieved, namely that EWPhT $(0, w_+) \to (v, 0)$ is the only PhT in our model, with T_c being the critical temperature at which the two minima become degenerate. Thirdly, in order to make sure that the EWPhT completes, we conservatively require that, below $T = 50$ GeV, the only remaining minimum is the EW minimum. Lastly, we always choose the singlet mass to be more than half the Higgs mass, $m_\eta > \frac{m_h}{2}$, so as to kinematically close the dangerous $h \to \eta\eta$ decay channel, which is tightly constrained by Higgs decay width measurements [17, 18].

The graphical representation of these constraints is shown in Fig. 1, where in the left (right) panel we fix $\lambda_{h\eta} = 0.1$, $m_\eta = 75$ GeV and vary λ_η and Λ (fix $m_\eta = 75$ GeV, $\Lambda = 1.5$ TeV and vary $\lambda_{h\eta}$ and λ_η). The coloured regions are excluded by the constraints listed above, with the allowed region remaining white. It is interesting to note from the figure that, in our scenario, all the free parameters lie within bounded intervals. Most notably, the value of the scale of New Physics Λ is bounded from above, demonstrating the crucial role of the $D = 6$ operator.
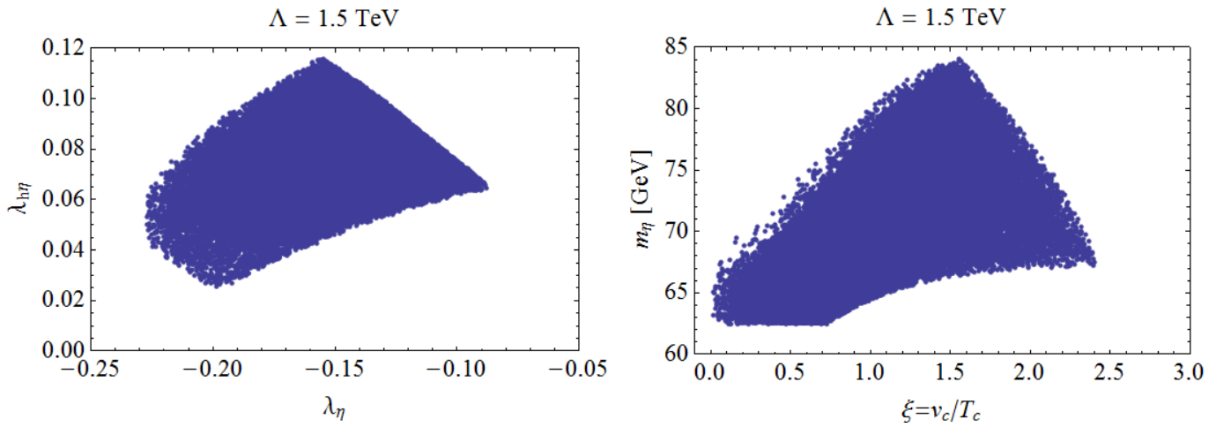
Figure 2. Values of the parameters for which a one–step (S)FOEWPhT occurs. The cutoff of the dimension–6 operator has been set to $\Lambda = 1.5$ TeV.

In a second stage of our numerical analysis, we fix $\Lambda = 1.5$ TeV and then scan over the remaining three free parameters, λ_η, $\lambda_{h\eta}$, and m_η, at the same time imposing the constraints discussed previously. For each viable parameter point, we then calculate the critical temperature T_c corresponding to the $(0, w_+) \to (v, 0)$ FOEWPhT, and evaluate the EWPhT strength as $\xi = v(T_c)/T_c$. We show the results of our scan in the scatter plots in Fig. 2 and find that a SFOEWPhT (with $\xi > 1.3$), vital for EWBG, can be accommodated. We see that relatively small (absolute) values of the quartic and portal couplings are preferred to arrive at the desired thermal history, as opposed to the Z_2 symmetry–restoring scenario from Ref. [19], which favors $\mathcal{O}(1)$ values.[4] Qualitatively speaking, the singlet quartic in the Z_2–restoring case gets pushed to higher values by imposing that the EW minimum is deeper than the Z_2–breaking one at $T = 0$:

$$-\frac{\mu_\eta^4}{\lambda_\eta} > -\frac{\mu_h^4}{\lambda_h} \;\Rightarrow\; \lambda_\eta > \lambda_h \frac{\mu_\eta^4}{\mu_h^4}. \tag{2.10}$$

However, imposing the same condition in our Z_2 SNR case gives an upper bound on the absolute value of λ_η,

$$|\lambda_\eta|^3 < \text{const} \times \frac{\lambda_h v^4}{\Lambda^4}, \tag{2.11}$$

which follows from the depth of the two minima scaling (for negative λ_η) as

$$-V(v, 0, 0) \sim \lambda_h v^4, \quad -V(0, w_+, 0) \sim |\lambda_\eta| \, w_+^4 \sim |\lambda_\eta|^3 \, \Lambda^4. \tag{2.12}$$

Furthermore, the singlet is predicted to be rather light, with mass below ~ 85 GeV.

Lastly, in Figs 3 and 4, we show the thermal history of the Universe for a benchmark point given by $\lambda_\eta = -0.15$, $\lambda_{h\eta} = 0.1$, $m_\eta = 75$ GeV, and $\Lambda = 1.5$ TeV. At

---

[4]Small portal couplings could also be interesting for potential realizations of dark matter in the singlet-extended SM.
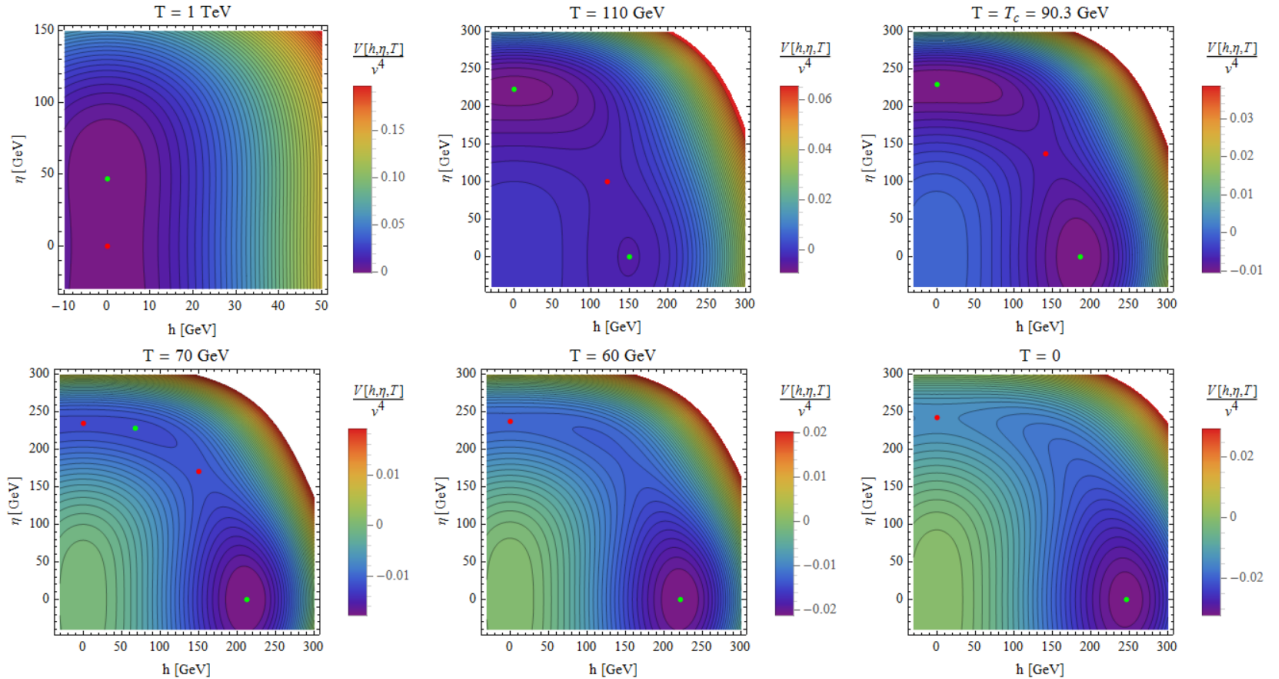
Figure 3. Thermal evolution of the potential for a benchmark point with $\lambda_\eta = -0.15$, $\lambda_{h\eta} = 0.1$, and $m_\eta = 75$ GeV. The green dots denote local and global minima, whereas the red dots represent saddle points. The cutoff of the dimension–6 operator has been set to $\Lambda = 1.5$ TeV.

very high temperatures, the Universe starts in a EW–symmetric phase with broken Z_2 symmetry (upper left panel in Fig. 3). As the plasma cools down, the EW minimum starts to develop, and is separated from the EW–symmetric minimum by a barrier (upper central panel). Once the critical temperature is attained and the two minima become degenerate (upper right panel), bubbles of the EW–broken phase start to nucleate and the SFOEWPhT proceeds. At a certain temperature below T_c, the false vacuum at $(0, w_+)$ turns into a saddle point, and the local minimum at (v_{b_+}, w_{b_+}) starts to develop [5] in its place (lower left panel). Later on, at even lower temperatures, the local minimum at (v_{b_+}, w_{b_+}) and the barrier disappear (lower central panel), leaving the EW minimum as the only minimum all the way to $T = 0$ (lower right panel).

The thermal history of our model is plotted and confronted with the standard Z_2-restoring case in Fig. 4. Here, we show the T-dependent evolution of the doublet and singlet vevs for the mentioned benchmark (solid lines), and compare it to the conventional case where higher-dimensional operators are neglected (dashed

---

[5]This opens up the curious possibility of the minimum at (v_{b_+}, w_{b_+}) appearing before the $(0, w_+) \to (v, 0)$ phase transition completes, which would result in nucleation and collision of bubbles of the broken EW phase in a time–varying background. However, investigating such a scenario is beyond the scope of the present work.
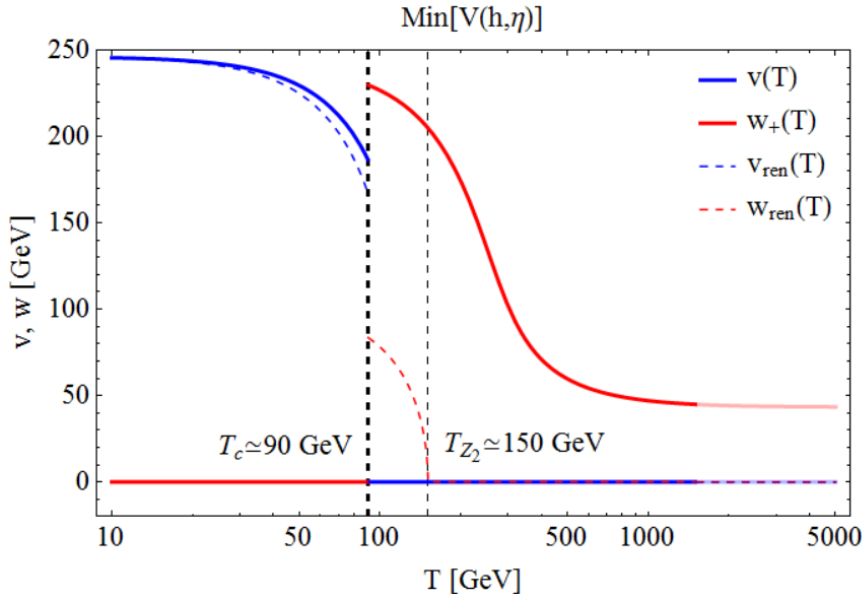
Figure 4. Thermal evolution of the doublet and singlet vevs in our model for the benchmark point with $\lambda_\eta = -0.15$, $\lambda_{h\eta} = 0.1$, $m_\eta = 75$ GeV, and $\Lambda = 1.5$ TeV (solid lines), compared to the conventional case where higher-dimensional operators are neglected (dashed lines), assuming the same critical temperature $T_c \simeq 90$ GeV. The latter features the characteristic two-step breaking pattern, with Z_2 breaking at $T_{Z_2} > T_c$. The region where the validity of the considered EFT starts to break down ($T > \Lambda$) is visualized by faint lines.

lines), assuming the same critical temperature $T_c \simeq 90$ GeV. The latter features the characteristic two-step breaking pattern, with potentially dangerous Z_2 breaking at $T_{Z_2} > T_c$, which can be avoided in the case at hand which features a saturating finite w_+ at high temperatures.

3 SO(6)/SO(5) Composite Higgs Realization

Here, we present a minimal UV completion of the EFT discussed above in the form of a $SO(6)/SO(5)$ CH model. The extended scalar sector of this nMCHM [2] contains in fact a pseudoscalar pseudo Nambu-Goldstone boson (pNGB) singlet S in addition to the pNGB EW Higgs doublet H. Following the partial-compositeness (PC) paradigm [20–23], elementary (SM-like) quarks q_L, q_R are coupled to the composite fermionic resonances via linear mixings that explicitly break the global $SO(6)$ symmetry and induce a potential $V(H, S)$ for the scalars, which sensitively depends on the choice of $SO(6)$ representations for the composite matter sector. A main result of this section will be a comprehensive overview of the form of this potential, being a crucial ingredient for EWBG, for the various possible $SO(6)$ representations of the composite fermions in the $SO(6)/SO(5)$ CH, complementing and systematically completing the results available in the literature [2, 19, 24–26].

While EWBG can work in the nMCHM, in the literature so far a specific thermal history with a two-step breaking pattern of $(0,0) \to (0,w) \to (v,0)$ in scalar field space was investigated [3, 19, 25, 26], realized in a part of the parameter space of the nMCHM. Since, as explained before, such a transition pattern could be problematic, here we will focus on an alternative region, that can allow for the distinct thermal history lined out in Section 2 (which would also be interesting on its own right, beyond the question of emerging topological defects). This space will emerge just by allowing for negative λ_η and considering $D > 4$ operators in the Higgs potential, that automatically appear in the CH framework.

In order to identify setups that feature the structure of couplings envisaged in Section 2, we employ a spurion analysis where we formally restore the $SO(6)$-invariance in the linear mixings by uplifting the elementary fermions to transform under the full $SO(6)$ symmetry, even though they actually correspond to incomplete $SO(6)$ multiplets. The spurious symmetry can then be used to constrain the form of the scalar potential.

3.1 General Setup

We start by specifying the CH framework.[6] Schematically, the Lagrangian below the compositeness scale Λ_c, where the substructure of the scalars would be revealed, reads (after integrating out the heavy resonances)

$$\mathcal{L}_{\text{CH}} \supset \mathcal{L}_{\text{kin}}^{H,S} + \mathcal{L}_{\text{Yukawa}} + \mathcal{L}_{WZW} - V(H, S). \tag{3.1}$$

Here, $\mathcal{L}_{\text{kin}}^{H,S}$ denotes the kinetic term for the scalars, $\mathcal{L}_{\text{Yukawa}}$ contain the light-fermion Yukawa couplings originating from PC, and $\mathcal{L}_{WZW}$ are Wess-Zumino-Witten (WZW) couplings of the singlet to gauge bosons (which will play no role in the following). The relevant terms, and in particular the Higgs potential $V(H, S)$, will be discussed below. We are especially interested in $D = 6$ corrections to the latter to support the SNR scenario of Section 2. For this purpose, we will analyze several different PC scenarios. We will concentrate on the top sector $q_L = (t_L, b_L)$, $q_R = t_R$ in particular, but an equivalent analysis can be done for all other quarks. Furthermore, we neglect the gauge boson contribution (which is usually much smaller).

We denote the 15 generators of $SO(6)$ as $T^A = \{T^{\bar{A}}, \hat{T}_6^r\}$, with $T^{\bar{A}} = \{T_L^a, T_R^a, T_5^i\}$ being the 10 generators of $SO(5)$, where T_L^a, T_R^a correspond to the $SU(2)_L, SU(2)_R$ subgroups, respectively. On the other hand, $\hat{T}_6^r$ are the 5 broken generators of $SO(6)/SO(5)$, containing a $SU(2)_L \times SU(2)_R$ bi-doublet ($r = 1, \dots, 4$) and a singlet

---

[6]For a more complete introduction on $SO(6)/SO(5)$ CH models, see, e.g., [2, 3, 19, 24–28].

$(r = 5)$. They can be written as [25, 28]

$$\left[T_L^a\right]_{IJ} = -\frac{\imath}{2}\left[\frac{1}{2}\epsilon^{abc}\left(\delta_{bI}\delta_{cJ} - \delta_{bJ}\delta_{cI}\right) + \left(\delta_{aI}\delta_{4J} - \delta_{aJ}\delta_{4I}\right)\right]$$

$$\left[T_R^a\right]_{IJ} = -\frac{\imath}{2}\left[\frac{1}{2}\epsilon^{abc}\left(\delta_{bI}\delta_{cJ} - \delta_{bJ}\delta_{cI}\right) - \left(\delta_{aI}\delta_{4J} - \delta_{aJ}\delta_{4I}\right)\right]$$

$$\left[T_5^i\right]_{IJ} = -\frac{\imath}{\sqrt{2}}\left(\delta_{iI}\delta_{5J} - \delta_{iJ}\delta_{5I}\right)$$

$$\left[\hat{T}_6^r\right]_{IJ} = -\frac{\imath}{\sqrt{2}}\left(\delta_{rI}\delta_{6J} - \delta_{rJ}\delta_{6I}\right)\,,$$

(3.2)

where $a = 1,2,3$, $i = 1,\ldots,4$, $r = 1,\ldots,5$ and $I,J = 1,\ldots,6$. Note that we will need an additional $U(1)_X$ to reproduce the correct hypercharge $Y = X + T_R^3$ for the SM gauge group. The Goldstone matrix, encoding the dynamics of the pNGBs, is defined as

$$U\left[\vec{\Pi}\right] = \exp\left(\imath\frac{\sqrt{2}}{f}\Pi_r\hat{T}_6^r\right)$$

(3.3)

with Π_r the five Goldstone modes and $f = \Lambda_c/(4\pi)$ the pseudo-Goldstone decay constant. Under $g \in SO(6)$, the Goldstone matrix transforms as (see, e.g., [29])

$$U\left[\vec{\Pi}\right] \to g \cdot U\left[\vec{\Pi}\right] \cdot \hat{h}^T\left[\vec{\Pi}; g\right]\,, \qquad \hat{h} = \begin{pmatrix} \hat{h}_5 & 0 \\ 0 & 1 \end{pmatrix}\,, \qquad \hat{h}_5 \in SO(5)\,,$$

(3.4)

providing the non-linear realization of the $SO(6)$-symmetry of the Π-fields that transform in the fundamental representation of $SO(5)$. Using the generators T_L^a, we can perform a $SU(2)_L$ gauge transformation such that

$$\vec{\Pi} = \left(\Pi_1, \Pi_2, \Pi_3, \Pi_4, \Pi_5\right)^T \overset{SU(2)_L}{\to} \left(0, 0, 0, \Pi_4, \Pi_5\right)^T\,,$$

(3.5)

where three Higgs degrees of freedom are eaten by the EW gauge bosons. However, using this parametrization would lead to a rather involved kinetic term involving trigonometric functions of Π_4 and Π_5 so we further redefine [2, 25]

$$\frac{h}{f} = \frac{\Pi_4}{\sqrt{\Pi_4^2 + \Pi_5^2}}\sin\frac{\sqrt{\Pi_4^2 + \Pi_5^2}}{f}, \quad \frac{S}{f} = \frac{\Pi_5}{\sqrt{\Pi_4^2 + \Pi_5^2}}\sin\frac{\sqrt{\Pi_4^2 + \Pi_5^2}}{f}$$

(3.6)

which is hereafter simply referred to as unitary gauge. This leads to the Goldstone matrix

$$U = \begin{pmatrix} \mathbb{I}_{3\times3} & & & \\ & 1 - \frac{h^2}{f^2 + f\sqrt{f^2 - h^2 - S^2}} & -\frac{hS}{f^2 + f\sqrt{f^2 - h^2 - S^2}} & \frac{h}{f} \\ & -\frac{hS}{f^2 + f\sqrt{f^2 - h^2 - S^2}} & 1 - \frac{S^2}{f^2 + f\sqrt{f^2 - h^2 - S^2}} & \frac{S}{f} \\ & -\frac{h}{f} & -\frac{S}{f} & \frac{1}{f}\sqrt{f^2 - h^2 - S^2} \end{pmatrix}$$

(3.7)

and the composite sector kinetic term [24]

$$\mathcal{L}_{\text{kin}}^{H,S} = \frac{f^2}{4} Tr(d_\mu d^\mu) = (D_\mu H)^\dagger D^\mu H + \frac{1}{2}(\partial_\mu S)^2 + \frac{1}{2f^2}\left[\partial_\mu(H^\dagger H) + \frac{1}{2}\partial_\mu S^2\right]^2 + \mathcal{O}\left(\frac{1}{f^4}\right),$$

$$(3.8)$$

where d_μ is the broken generator part of the Maurer-Cartan form $\omega_\mu = U^{-1}D_\mu U = d_{\mu\bar{A}}T^{\bar{A}} + e_{\mu A}T^A \equiv d_\mu + e_\mu$, and we rewrote the pNGB Higgs as a complex $SU(2)$ doublet with $H = \frac{1}{\sqrt{2}}(0,h)^T$ in unitary gauge.

3.2 Fermion Embeddings and Scalar Potential

Regarding the fermions, the simplest option for the right-handed SM quarks is to embed t_R in a singlet of $SO(6)$ (being either partially or fully composite), for which the potential only receives contributions from the spurions corresponding to the left-handed SM quarks, q_L, see below. Concerning higher representations, the spinorial **4** is not considered in general, as it does not obey custodial symmetry for the $Z\bar{b}b$ couplings [19]. On the other hand **10**-representations are neglected because they fail to produce a singlet potential as they do not break the $SO(2)_S \subset SO(6)$ subgroup [19], while the **20** and **20''** representations do not yield valid SM quark embeddings at all. Therefore, we consider combinations of $q_L \in (\mathbf{6}, \mathbf{15}, \mathbf{20'})$ and $t_R \in (\mathbf{1}, \mathbf{6}, \mathbf{15}, \mathbf{20'})$ [19, 25, 26].

The **6** decomposes under $SO(6) \times U(1)_X \rightarrow SO(5) \times U(1)_X \rightarrow SO(4) \times U(1)_X \rightarrow SU(2) \times U(1)_Y$ as

$$\begin{aligned}
\mathbf{6}_{2/3} &\rightarrow \mathbf{5}_{2/3} \oplus \mathbf{1}_{2/3} \\
&\rightarrow \left[\mathbf{4}_{2/3} \oplus \mathbf{1}_{2/3}\right] \oplus \mathbf{1}_{2/3} \\
&\rightarrow \left[\left(\mathbf{2}_{7/6} \oplus \mathbf{2}_{1/6}\right) \oplus \mathbf{1}_{2/3}\right] \oplus \mathbf{1}_{2/3}.
\end{aligned}$$

As there is only one $\mathbf{2}_{1/6}$, the Q_L embedding in $SO(6)$ is unique, while t_R resides in a superposition of the two $\mathbf{1}_{2/3}$, parameterized by the angle θ_{6R}:

$$Q_L^6 = \frac{1}{\sqrt{2}}\left((Q_L^4)^T\ 0\ 0\right)^T, \quad t_R^6 = \left(0\ 0\ 0\ 0\ t_R e^{i\phi_{6R}}\cos\theta_{6R}\ t_R\sin\theta_{6R}\right)^T, \quad (3.9)$$

where $Q_L^4 = \left(i b_L\ b_L\ i t_L\ -t_L\right)^T$. In the following we employ $\phi_{6R} = \pm\pi/2$, in agreement with a CP-conserving top coupling [27]. For our purposes, we want to avoid $\theta_{6R} = \pm\pi/4$, for which the singlet stays a pure Goldstone. The angle $\theta_{6R} = \pm\pi/2$ on the other hand yields a Z_2 symmetry with the singlet being odd, making it a dark matter candidate [27], but we will not explore this direction further here.

The **15** decomposes as

$$
\begin{aligned}
\mathbf{15}_{2/3} &\to \mathbf{10}_{2/3} \oplus \mathbf{5}_{2/3} \\
&\to \left[\mathbf{3}_{2/3} \oplus \mathbf{3}'_{2/3} \oplus \mathbf{4}_{2/3}\right] \oplus \left[\mathbf{4}_{2/3} \oplus \mathbf{1}_{2/3}\right] \\
&\to \left[\mathbf{3}_{2/3} \oplus \left(\mathbf{1}_{5/3} \oplus \mathbf{1}_{2/3} \oplus \mathbf{1}_{-1/3}\right) \oplus \left(\mathbf{2}_{7/6} \oplus \mathbf{2}_{1/6}\right)\right] \oplus \left[\left(\mathbf{2}_{7/6} \oplus \mathbf{2}_{1/6}\right) \oplus \mathbf{1}_{2/3}\right].
\end{aligned}
$$

Thus, q_L can be embedded in the **10** (A) or the **5** (B) of $SO(5)$,

$$
Q_L^{15\mathrm{A}} = (Q_L^4)_j T_5^j, \quad Q_L^{15\mathrm{B}} = \imath (Q_L^4)_j \hat{T}_6^j. \tag{3.10}
$$

A general embedding would be given by

$$
Q_L^{15} = \cos\theta_{15L} e^{\imath\phi_{15L}} Q_L^{15\mathrm{A}} + \sin\theta_{15L} Q_L^{15\mathrm{B}}, \tag{3.11}
$$

however, since $\mathbf{15}_\mathrm{B}$ is heavily constrained by $Zb\bar{b}$ couplings [25] it is dropped below, corresponding to $\theta_{15L} = 0$. Similarly, the t_R can be embedded as

$$
t_R^{15} = \cos\theta_{15R} e^{\imath\phi_{15R}} T_R^3 t_R + \sin\theta_{15R} \hat{T}_6^5 t_R. \tag{3.12}
$$

Finally, the $\mathbf{20}'$ decomposes as

$$
\begin{aligned}
\mathbf{20}'_{2/3} &\to \mathbf{14}_{2/3} \oplus \mathbf{5}_{2/3} \oplus \mathbf{1}_{2/3} \\
&\to \left[\mathbf{9}_{2/3} \oplus \mathbf{4}_{2/3} \oplus \mathbf{1}_{2/3}\right] \oplus \left[\mathbf{4}_{2/3} \oplus \mathbf{1}_{2/3}\right] \oplus \mathbf{1}_{2/3} \\
&\to \left[\left(\mathbf{3}_{5/3} \oplus \mathbf{3}_{2/3} \oplus \mathbf{3}_{-1/3}\right) \oplus \left(\mathbf{2}_{7/6} \oplus \mathbf{2}_{1/6}\right) \oplus \mathbf{1}_{2/3}\right] \oplus \left[\left(\mathbf{2}_{7/6} \oplus \mathbf{2}_{1/6}\right) \oplus \mathbf{1}_{2/3}\right] \oplus \mathbf{1}_{2/3},
\end{aligned}
$$

and we can write $Q_L^{20'}$ as a superposition of the embeddings in a **14** (A) and a **5** (B) of SO(5),

$$
Q_L^{20'_\mathrm{A}} = \frac{1}{2}\begin{pmatrix} 0_{4\times4} & Q_L^4 & 0_{4\times1} \\ (Q_L^4)^T & 0 & 0 \\ 0_{1\times4} & 0 & 0 \end{pmatrix}, \quad Q_L^{20'_\mathrm{B}} = \frac{1}{2}\begin{pmatrix} 0_{4\times4} & 0_{4\times1} & Q_L^4 \\ 0_{1\times4} & 0 & 0 \\ (Q_L^4)^T & 0 & 0 \end{pmatrix}, \tag{3.13}
$$

with a general realization given by

$$
Q_L^{20'} = \cos\theta_{20L} e^{\imath\phi_{20L}} Q_L^{20'_\mathrm{A}} + \sin\theta_{20L} Q_L^{20'_\mathrm{B}}. \tag{3.14}
$$

While the $\mathbf{20}'_\mathrm{B}$ leads again to large corrections to $Zb\bar{b}$ [26], for most models considered, sticking to $Q_L^{20'_\mathrm{A}}$ would not lead to a phenomenologically viable model and we will keep the superposition, see below. Finally, t_R can be embedded in a superposition of the **14** (A), **5** (B) and **1** (C) representations,

$$
t_R^{20'_\mathrm{A}} = \frac{1}{2\sqrt{5}}\begin{pmatrix} -\mathbb{I}_{4\times4} t_R & 0_{4\times2} \\ 0_{2\times4} & 2(\mathbb{I}_{2\times2} + \sigma^3) t_R \end{pmatrix}, \quad t_R^{20'_\mathrm{B}} = \frac{1}{\sqrt{2}}\begin{pmatrix} 0_{4\times4} & 0_{4\times2} \\ 0_{2\times4} & \sigma^1 t_R \end{pmatrix},
$$

$$
t_R^{20'_\mathrm{C}} = \frac{1}{\sqrt{30}}\begin{pmatrix} -\mathbb{I}_{5\times5} t_R & 0_{5\times1} \\ 0_{1\times5} & 5 t_R \end{pmatrix}, \tag{3.15}
$$

where σ^a are the Pauli matrices, leading to

$$
t_R^{20'} = \cos\theta_{20R1} e^{\imath\phi_{20R1}} t_R^{20'_A} + \sin\theta_{20R1} \cos\theta_{20R2} e^{\imath\phi_{20R2}} t_R^{20'_B} + \sin\theta_{20R1} \sin\theta_{20R2} t_R^{20'_C}. \tag{3.16}
$$

3.2.1 Warm-Up: $(\mathbf{20'}, \mathbf{1})$ Minimally Extended SILH

As a first explicit example, we will evaluate the fermion couplings and the pNGB potential for the $(\mathbf{20'}, \mathbf{1})$ model with the Q_L in a $\mathbf{20'}$ of $SO(6)$ and a fully composite t_R singlet, allowing a viable EW symmetry breaking (EWSB) from leading (LO) order in the PC expansion [24]. Compared to the analyses available in the literature, here and below we will take into account higher orders in the scalar potential, which are crucial to reveal regions of parameter space allowing for the novel SNR thermal history. While we will follow the parametrization given above, the analysis is consistent with [24], which we will further comment on later. We can rewrite the general embedding in a $\mathbf{20'}$ of Eq. (3.14) as

$$\begin{aligned}
Q_L^{20'} &= \cos\theta_{20L} e^{i\phi_{20L}} Q_L^{20'_A} + \sin\theta_{20L} Q_L^{20'_B} \\
&= \Lambda_L^1 b_L + \Lambda_L^2 t_L = \Lambda_L^\alpha q_{L\alpha} \,,
\end{aligned} \tag{3.17}$$

where, abbreviating $\mathfrak{c}_\theta \equiv \cos\theta_{20L}$ and $\mathfrak{s}_\theta \equiv \sin\theta_{20L}$,

$$\Lambda_L^1 = \frac{1}{2} \begin{pmatrix} & & & & ie^{i\phi_{20L}}\mathfrak{c}_\theta & i\mathfrak{s}_\theta \\ & 0_{4\times4} & & & e^{i\phi_{20L}}\mathfrak{c}_\theta & \mathfrak{s}_\theta \\ & & & & 0 & 0 \\ & & & & 0 & 0 \\ ie^{i\phi_{20L}}\mathfrak{c}_\theta & e^{i\phi_{20L}}\mathfrak{c}_\theta & 0 & 0 & & \\ i\mathfrak{s}_\theta & \mathfrak{s}_\theta & 0 & 0 & 0_{2\times2} \end{pmatrix},$$

$$\Lambda_L^2 = \frac{1}{2} \begin{pmatrix} & & & & 0 & 0 \\ & 0_{4\times4} & & & 0 & 0 \\ & & & & ie^{i\phi_{20L}}\mathfrak{c}_\theta & i\mathfrak{s}_\theta \\ & & & & -e^{i\phi_{20L}}\mathfrak{c}_\theta & -\mathfrak{s}_\theta \\ 0 & 0 & ie^{i\phi_{20L}}\mathfrak{c}_\theta & -e^{i\phi_{20L}}\mathfrak{c}_\theta & & \\ 0 & 0 & i\mathfrak{s}_\theta & -\mathfrak{s}_\theta & 0_{2\times2} \end{pmatrix}, \tag{3.18}$$

provide the $SO(6)$ embeddings of the left-handed bottom and top sector, respectively.

As mentioned in the beginning of this section, we assume PC for the coupling of the SM to the composite sector, i.e. we couple the multiplets above to composite fermion resonances $\Psi^{T,t}$ linearly. For the following discussion, and in particular for the construction of the pNGB Higgs potential, it is useful to lift the SM fermions to (spurious) $SO(6)$ multiplets by assigning the embedding matrices Λ_L^i transformation properties under the full $SO(6)$ global symmetry in an intermediate step, making them so-called spurions of $SO(6)$. This allows to construct the Lagrangian with the help of the spurions from symmetry principles, i.e. an $SO(6)$ symmetry explicitly broken only by setting the spurions back to their actual background values of (3.18) in the end. Moreover, it is convenient to construct the $SO(6)$-Lagrangian in terms of $SO(5)$ objects as per the CCWZ construction [29–31]: Using the transformation

properties of U in (3.4), we can construct the dressed embedding matrices,

$$(\Lambda_L'^{\alpha})_{66} = (U^T)_{6I}(U^T)_{6J}(\Lambda_L^{\alpha})^{IJ}, \tag{3.19}$$

$$(\Lambda_L'^{\alpha})_{a6} = (U^T)_{aI}(U^T)_{6J}(\Lambda_L^{\alpha})^{IJ}, \tag{3.20}$$

$$(\Lambda_L'^{\alpha})_{ab} = (U^T)_{aI}(U^T)_{bJ}(\Lambda_L^{\alpha})^{IJ}, \tag{3.21}$$

where $a, b = 1, \ldots, 5$, obtaining $SO(5)$-singlets, fiveplets and **14**-plets[7], and the resonances can be split similarly. We then build a formally $SO(5)$ and thus, by virtue of U, $SO(6)$ invariant Langrangian, only broken by the spurions aqcuiring their background values. The PC Lagrangian then reads [26]

$$\mathcal{L}_{\text{PC}} = -y_L f\left(a(\bar{\Psi}_R^{T\prime})^{66}(\Lambda_L'^{\alpha})_{66} + b(\bar{\Psi}_R^{T\prime})^{6a}(\Lambda_L'^{\alpha})_{a6} + c(\bar{\Psi}_R^{T\prime})^{ab}(\Lambda_L'^{\alpha})_{ba}\right) q_{L\alpha} + \text{h.c.}, \tag{3.22}$$

where a, b, c are $\mathcal{O}(1)$ numbers.

To arrive at the low energy Yukawa Lagrangian $\mathcal{L}_{\text{Yukawa}}$, one could integrate out the resonances, yielding form factors, as considered e.g. in [25, 26]. Alternatively, as explained, one can just construct $SO(5)$ invariants from only the SM fields, spurions and the Goldstone matrix to obtain $\mathcal{L}_{\text{Yukawa}}$, where the heavy field contributions are absorbed. The Yukawa Lagrangian then reads (up to $\mathcal{O}(1)$ proportionality factors that will drop out in (3.24) below)

$$\begin{aligned}
\mathcal{L}_{\text{Yukawa}} &= y_L f\, \bar{t}_R(\Lambda_L'^{\alpha})_{66} q_{L\alpha} + \text{h.c.} \\
&= y_L\, \bar{t}_R \frac{1}{f}\left(-h\sqrt{f^2 - h^2 - S^2}\sin\theta_{20\text{L}} + \imath h S \cos\theta_{20\text{L}}\right) t_L + \text{h.c.} \\
&= -\sqrt{2}y_L\, \bar{q}_L H^c t_R \sin\theta_{20\text{L}}\left(1 - \frac{|H|^2}{f^2} - \frac{S^2}{2f^2} + \mathcal{O}\left(\frac{1}{f^4}\right)\right) \\
&\quad - \imath\sqrt{2}y_L \cos\theta_{20\text{L}}\frac{S}{f}\bar{q}_L H^c t_R + \text{h.c.}.
\end{aligned} \tag{3.23}$$

To make S a real, CP-odd scalar, guaranteeing a Z_2-symmetric form of the potential, we chose $\phi_{20\text{L}} = -\pi/2$ in the second row and in the last row $H^c = \imath\sigma_2 H^* = \frac{1}{\sqrt{2}}(h, 0)^T$ in unitary gauge. We identify $y_t \equiv \sqrt{2}y_L \sin\theta_{20\text{L}}$ as the (LO) SM top-Higgs coupling and $\epsilon_Q \equiv \cot\theta_{20\text{L}}$ as the mixing parameter of the embedding, such that, in agreement with [24],

$$\mathcal{L}_{\text{Yukawa}} = \frac{y_t}{\sqrt{2}}\bar{t}_R \frac{1}{f}\left(-h\sqrt{f^2 - h^2 - S^2} + \imath\epsilon_Q h S\right) t_L + \text{h.c.}. \tag{3.24}$$

Summarizing the results so far in the latter parametrization (including the other terms of Eq. (3.1)) and generalizing them to three quark families ($i, j = 1, ..3$) we

---

[7]The bottom-spurion singlet vanishes in this configuration, related to the bottom quark being still massless. To account for a bottom mass, the embedding $Q_L^{20\prime}$ would have to be modified, c.f. [29], which would however not change our analysis notably.

obtain the effective Lagrangian for the model at hand, up to $D = 6$ (see also [24])

$$\mathcal{L}^{D \leq 6}_{(\mathbf{20'},1)} \supset (D_\mu H)^\dagger D^\mu H + \frac{1}{2}(\partial_\mu S)^2 + \frac{1}{2f^2}\left[\partial_\mu |H|^2 + \frac{1}{2}\partial_\mu S^2\right]^2$$

$$- \sum_{q_R = u_R, d_R} (y_q)_{ij} \bar{q}_L^i H q_R^j \left(1 + i\epsilon_Q^i \frac{S}{f} - \frac{1}{f^2}(|H|^2 + S^2/2)\right) + \text{h.c.} \qquad (3.25)$$

$$+ \frac{S}{16\pi^2 f}\left[n_B B_{\mu\nu}\tilde{B}^{\mu\nu} + n_W W^{I\mu\nu}\tilde{W}^I_{\mu\nu} + n_G G^{a\mu\nu}\tilde{G}^a_{\mu\nu}\right] - V(H,S),$$

where $H \to H^c$ for $q_R = u_R$ in the second line. The first term in the last line corresponds to the WZW Lagragian, with the anomaly coefficients fixed by the coset (with $n_W = n_B, n_G = 0$ for $SO(6)/SO(5)$ [2]). These couplings supplement the SM-fermion loops mediating the same transitions, if coupled to S. We will now turn to the evaluation of the scalar potential $V(H,S)$.

We can finally construct the potential by using that it is proportional to explicit $SO(6)$ breaking effects, parameterized by the spurions Λ_L^α. Therefore, as mentioned before, we just build formally $SO(6)$ invariant terms consisting of the dressed spurions. Setting them to their background values of (3.18) will then lead to the actual scalar potential. Moreover, to ensure that the terms also respect the SM gauge group, we need an even number of spurions (saturating the SM index). Assuming a one-scale-one-coupling framework as described, e.g., in [24, 29, 32], we can determine the scaling of any potential term by dimensional analysis,

$$V \propto N_C \frac{m_*^4}{g_*^2}\left(\frac{\hbar g_*^2}{16\pi^2}\right)^{\#Loops}\left(\frac{y_{L/R}\Lambda}{g_*}\right)^{\#spurions}\left(\frac{h}{f}\right)^{\#h}\left(\frac{S}{f}\right)^{\#S}, \qquad (3.26)$$

where $m_* = g_* f$ is the resonance mass scale, with g_* the coupling of the composite sector, and N_C counts the QCD color multiplicity.

The (one-loop) invariants at LO in y_L read (setting $\hbar = 1$)

$$c_{\text{s2}}\frac{N_C m_*^4}{16\pi^2}\frac{y_L^2}{g_*^2}(\Lambda_L'^\alpha)_{66}(\Lambda_L'^{\alpha\dagger})^{66} = c_{\text{s2}}\frac{N_C g_*^2 y_L^2}{16\pi^2}\left(h^2\left(f^2 - h^2 - S^2\right)\mathfrak{s}_\theta^2 + h^2 S^2 \mathfrak{c}_\theta^2\right), \quad (3.27)$$

$$c_{\text{f2}}\frac{N_C m_*^4}{16\pi^2}\frac{y_L^2}{g_*^2}(\Lambda_L'^\alpha)_{a6}(\Lambda_L'^{\alpha\dagger})^{a6} = c_{\text{f2}}\frac{N_C g_*^2 y_L^2}{16\pi^2}\left(f^4 \mathfrak{s}_\theta^2 + \frac{f^2}{4}h^2(\mathfrak{c}_\theta^2 - 7\mathfrak{s}_\theta^2) + h^4 \mathfrak{s}_\theta^2\right.$$

$$\left. - h^2 S^2(\mathfrak{c}_\theta^2 - \mathfrak{s}_\theta^2) + f^2 S^2(\mathfrak{c}_\theta^2 - \mathfrak{s}_\theta^2)\right),$$

where the parameters $c_i \sim \mathcal{O}(1)$ encode the high energy dynamics and we chose a writing easily comparable with the ϵ_Q parametrization used in Ref. [24].[8] This results

---

[8]Note that the 14-plet is not included as, due to U being unitary, it does not induce linearly independent terms.

in the LO potential

$$V(h, S) = \frac{N_C g_*^2 y_L^2}{16\pi^2} \left(h^2 f^2 \left[c_{s2} \mathfrak{s}_\theta^2 + \frac{c_{f2}}{4} \left(\mathfrak{c}_\theta^2 - 7\mathfrak{s}_\theta^2 \right) \right] - h^4 \mathfrak{s}_\theta^2 \left(c_{s2} - c_{f2} \right) \right.$$
$$\left. + h^2 S^2 \left[\left(c_{s2} - c_{f2} \right) \left(\mathfrak{c}_\theta^2 - \mathfrak{s}_\theta^2 \right) \right] + S^2 f^2 c_{f2} \left(\mathfrak{c}_\theta^2 - \mathfrak{s}_\theta^2 \right) \right). \tag{3.28}$$

We can in turn identify the Higgs mass and quartic-coupling, μ and λ, which allows us to replace the UV parameters c_i below by connecting them to physical values at low energies. Note that no quartic S interaction is induced at LO in the spurion expansion. Minimizing with respect to h and S yields the $T = 0$ vevs

$$\langle h \rangle \equiv v = \frac{f}{2\sqrt{2}} \sqrt{\frac{4\mathfrak{s}_\theta^2 c_{s2} + c_{f2} \left(\mathfrak{c}_\theta^2 - 7\mathfrak{s}_\theta^2 \right)}{\mathfrak{s}_\theta^2 \left(c_{s2} - c_{f2} \right)}} = \sqrt{\frac{-\mu^2}{\lambda}}, \quad \langle S \rangle = 0 \tag{3.29}$$

where we already wrote v in terms of μ and λ. Employing $|H| = h/\sqrt{2}$ (in unitary gauge) finally leads to

$$V(H, S) = \mu^2 |H|^2 + \lambda |H|^4 + \lambda f^2 \left(1 - 2\frac{v^2}{f^2} \right) \left(\frac{\epsilon_Q^2 - 1}{\epsilon_Q^2 - 3} \right) S^2$$
$$- \frac{1}{2} (\epsilon_Q^2 - 1) \lambda S^2 |H|^2 . \tag{3.30}$$

Note that, having reverted to the ϵ_Q parametrization, our result agrees with the one of Ref. [24]. For $\epsilon_Q^2 = 1$, the singlet becomes an exact Goldstone boson, making it massless and not entering the scalar potential.

Higher orders in the potential

To explore if we can obtain a S^6 (and S^4) term in the model at hand, required for Z_2 SNR, in the following we inspect the invariants arising at higher order in spurion insertions (i.e., higher order in y_L). At next-to-leading order (NLO) and NNLO, in addition to naive powers of LO terms, we need to consider the new structures[9]

$$\tilde{c}_{f4} \frac{N_C m_*^4}{16\pi^2} \frac{y_L^4}{g_*^4} (\Lambda_L'^\alpha)_{a6} (\Lambda_L'^{\beta\dagger})^{a6} (\Lambda_L'^\beta)_{b6} (\Lambda_L'^{\alpha\dagger})^{b6} ,$$
$$c_{sfsf} \frac{N_C m_*^4}{16\pi^2} \frac{y_L^4}{g_*^4} (\Lambda_L'^\alpha)_{66} (\Lambda_L'^{\beta\dagger})^{66} (\Lambda_L'^\beta)_{b6} (\Lambda_L'^{\alpha\dagger})^{b6} ,$$
$$\tilde{c}_{f6} \frac{N_C m_*^4}{16\pi^2} \frac{y_L^6}{g_*^6} (\Lambda_L'^\alpha)_{a6} (\Lambda_L'^{\beta\dagger})^{a6} (\Lambda_L'^\beta)_{b6} (\Lambda_L'^{\gamma\dagger})^{b6} (\Lambda_L'^\gamma)_{c6} (\Lambda_L'^{\alpha\dagger})^{c6} , \tag{3.31}$$

---

[9]We denote the coefficients of terms with n powers of the singlet and m powers of the $SO(5)$ fundamental by a subscript snf$m$. For untilded coefficients, multiplets with adjacent indices are $SU(2)_L$ contracted, while tilded ones correspond to the other possible contraction.

as well as corresponding combinations. For simplicity, we present here only the leading contributions for each operator. The resulting potential reads

$$\frac{16\pi^2}{N_C m_*^4} V[h, S] = \tilde{\mu}_h h^2 + \tilde{\mu}_S S^2 + \tilde{\lambda}_{h4} h^4 + \tilde{\lambda}_{h2S2} h^2 S^2 + \tilde{\lambda}_{S4} S^4$$
$$+ \tilde{\lambda}_{h6} h^6 + \tilde{\lambda}_{h4S2} h^4 S^2 + \tilde{\lambda}_{h2S4} h^2 S^4 + \tilde{\lambda}_{S6} S^6 + \mathcal{O}((h, S)^8) \quad (3.32)$$

$$\tilde{\mu}_h = \frac{y_L^2}{g_*^2} \frac{1}{f^2} \left[\mathfrak{s}_\theta^2 c_{\mathrm{s}2} + \left(\mathfrak{c}_\theta^2 - 7\mathfrak{s}_\theta^2\right) \frac{c_{\mathrm{f}2}}{4} \right]$$

$$\tilde{\mu}_S = \frac{y_L^2}{g_*^2} \frac{1}{f^2} \left(\mathfrak{c}_\theta^2 - \mathfrak{s}_\theta^2\right) c_{\mathrm{f}2}$$

$$\tilde{\lambda}_{h4} = -\frac{y_L^2}{g_*^2} \frac{1}{f^4} \mathfrak{s}_\theta^2 \left(c_{\mathrm{s}2} - c_{\mathrm{f}2}\right)$$

$$\tilde{\lambda}_{h2S2} = \frac{y_L^2}{g_*^2} \frac{1}{f^4} \left(\mathfrak{c}_\theta^2 - \mathfrak{s}_\theta^2\right) \left(c_{\mathrm{s}2} - c_{\mathrm{f}2}\right)$$

$$\tilde{\lambda}_{S4} = \frac{y_L^4}{g_*^4} \frac{1}{2f^4} \left(\mathfrak{c}_\theta^2 - \mathfrak{s}_\theta^2\right)^2 \left(2c_{\mathrm{f}4} + \tilde{c}_{\mathrm{f}4}\right)$$

$$\tilde{\lambda}_{h6} = \frac{y_L^4}{g_*^4} \frac{1}{4f^6} \mathfrak{s}_\theta^2 \Big[-8\mathfrak{s}_\theta^2 c_{\mathrm{s}4} - \left(\mathfrak{c}_\theta^2 - 11\mathfrak{s}_\theta^2\right) c_{\mathrm{s}2\mathrm{f}2}$$
$$+ 2\left(\mathfrak{c}_\theta^2 - 7\mathfrak{s}_\theta^2\right) c_{\mathrm{f}4} + 2\left(\mathfrak{c}_\theta^2 - 5\mathfrak{s}_\theta\right) \tilde{c}_{\mathrm{f}4} - \left(\mathfrak{c}_\theta^2 - 9\mathfrak{s}_\theta\right) c_{\mathrm{sfsf}} \Big]$$

$$\tilde{\lambda}_{h4S2} = \frac{y_L^4}{g_*^4} \frac{1}{4f^6} \left(\mathfrak{c}_\theta^2 - \mathfrak{s}_\theta^2\right) \Big[8\mathfrak{s}_\theta^2 c_{\mathrm{s}4} + \left(\mathfrak{c}_\theta^2 - 15\mathfrak{s}_\theta^2\right) c_{\mathrm{s}2\mathrm{f}2}$$
$$- 2\left(\mathfrak{c}_\theta^2 - 11\mathfrak{s}_\theta^2\right) c_{\mathrm{f}4} - 2\left(\mathfrak{c}_\theta^2 - 7\mathfrak{s}_\theta^2\right) \tilde{c}_{\mathrm{f}4} + \left(\mathfrak{c}_\theta^2 - 11\mathfrak{s}_\theta^2\right) c_{\mathrm{sfsf}} \Big]$$

$$\tilde{\lambda}_{h2S4} = \frac{y_L^4}{g_*^4} \frac{1}{2f^6} \left(\mathfrak{c}_\theta^2 - \mathfrak{s}_\theta^2\right)^2 \left(2c_{\mathrm{s}2\mathrm{f}2} - 4c_{\mathrm{f}4} - 2\tilde{c}_{\mathrm{f}4} + c_{\mathrm{sfsf}}\right)$$

$$\tilde{\lambda}_{S6} = \frac{y_L^6}{g_*^6} \frac{1}{4f^6} \left(\mathfrak{c}_\theta^2 - \mathfrak{s}_\theta^2\right)^3 \left(4c_{\mathrm{f}6} + 2\tilde{c}_{\mathrm{f}2\mathrm{f}4} + \tilde{c}_{\mathrm{f}6}\right) ,$$

extending the results of [24], where we chose again a form that allows for easy translation to the ϵ_Q parametrization. We thus find that the S^4 and S^6 terms are indeed generated at orders $(y_L/g_*)^4$ and $(y_L/g_*)^6$, respectively. However, this significant suppression is in tension with a straightforward realization of the SNR scenario and in particular lead to a too large EFT suppression Λ, see Section 2 and Section 4 below. We thus turn to an exploration of the other embeddings mentioned earlier to analyze if the suppression can get lifted.

3.2.2 Survey of Different Embeddings

In this section we will follow the procedure of Section 3.2.1 to calculate the potential for various fermion embeddings, aiming to carve out differences in the hierarchies of

couplings. Note that in the general case we get contributions from the t_R-spurions, too. We will thus distinguish between y_L and y_R-type spurions with

$$y_t \propto \frac{y_R y_L}{g^*}, \tag{3.33}$$

as per the definition of $\mathcal{L}_{\text{Yukawa}}$, see Appendix A, where the Yukawa terms for the realizations chosen below are given.

In Table 1-4 we provide an overview of the spurion-order at which the different terms in the potential appear for various viable combinations of q_L and t_R embeddings. We only take into account embeddings featuring no explicit CP-breaking, i.e. that only generate even powers of the pseudoscalar S in the potential, which basically fixes our choices for the angles ϕ_i below. In $\mathcal{L}_{\text{Yukawa}}$, a non-zero top mass as well as a CP-violation (CPv) inducing term $\propto \imath S h \bar{t} \gamma^5 t$ need to arise, the latter due to the last Sakharov criterion, constraining the viable embeddings further.[10] To minimize corrections to $Zb\bar{b}$, we restrict ourselves to $\mathbf{15}_{\text{A}L}$ ($\theta_{15L} = 0$) and assume $\langle S \rangle|_{T=0} = 0$ (c.f. [25]). A similar argument could be made for the $\mathbf{20}'_L$ [26], which we however only apply for the $(\mathbf{20}'_{\text{A}L}, \mathbf{20}'_R)$ since elsewhere it is in severe conflict with the more general constraints above (generating no top mass). Note that wherever we display only a limit $\theta_{L/R} = 0$, going to finite values of the angle does not change the hierarchy of the terms, except for the $(\mathbf{20}'_L, \mathbf{6}_R)$ where one particular choice – discussed below – leads to a vanishing S-potential. Finally, we will assess whether the respective models fit the SNR scenario of Section 2.

We start in Table 1 with the models where the t_R is realized as a composite singlet. Here, only Q_L in a $\mathbf{20}'_L$ yields a viable setup, with the results already discussed in Section 3.2.1. They are summarized here again for completeness with a slightly different ordering, using $\phi_{20L} = -\pi/2$, while $\theta_{20L} \neq \{0, \frac{\pi}{2}\}$ ensures a nonzero top-quark mass and the presence of CPv (and similarly for the following tables). For the $\mathbf{6}_L$, no singlet potential is generated as the embedding does not break the singlet shift symmetry, whereas for the $\mathbf{15}_L$ the top quark remains massless. For the $(\mathbf{20}'_L, \mathbf{1}_R)$ model, as discussed before, the singlet sextic (quartic) interaction is generated at order $(y_L/g_*)^6$ $((y_L/g_*)^4)$, making it challenging to realize the Z_2 SNR scenario with natural $\mathcal{O}(1)$ dimensionless coefficients. We finally note that both the renormalizable scalar portal as well as the pure ($D \leq 4$) Higgs terms arise at LO in spurions.

Next, we consider the models with a $\mathbf{6}_R$ embedding in Table 2. For the $(\mathbf{6}_L, \mathbf{6}_R)$ case, $\phi_{6R} = -\pi/2$ ensures a CP-conserving potential. Despite the fact that no CPv inducing term arises for $(\mathbf{15}_L, \mathbf{6}_R)$, we still write down (in gray font) the model for

---

[10]In the EFT of Section 2, with η a pseudoscalar, the necessary CP violation could be injected via a $(D=6)$ $\imath S^2 h \bar{t} \gamma^5 t$ operator [9]. We note that, even though the CH model features in general only a (spontaneously broken) CP symmetry and no additional Z_2, regarding the discussed thermal evolution both setups are equivalent.

$\theta_{15L} = 0$, and $\phi_{6R} - \phi_{15L} = \pi/2$. The $(\mathbf{20}'_L, \mathbf{6}_R)$ fulfills all conditions for $\phi_{20L} = -\pi/2$, $\phi_{6R} = \pi/2$. For simplicity, we choose $\theta_{6R} = 0$, as it generates a larger mass term for small θ_{20L} than the other naive limit $\theta_{6R} = \pi/2$, see Appendix A. Although this is not obvious from the table, for $\theta_{6R} = \pi/4$ and $\theta_{20L} = \pi/4$, the singlet becomes a true Goldstone boson in the $(\mathbf{20}'_L, \mathbf{6}_R)$ model, as is the case for the $(\mathbf{6}_L, \mathbf{6}_R)$. For all other cases, as before the S^n terms arise at the nth order in spurions. On the other hand, besides for the $(\mathbf{20}'_L, \mathbf{6}_R)$, the renormalizable portal and the Higgs quartic coupling emerge only at NLO in spurions, and are thus generically suppressed, while the Higgs mass term arises at LO. The latter hierarchy is relevant for the fine-tuning of the model, see e.g. [33–35].

The models with a $\mathbf{15}_R$ are displayed in Table 3. As the $\mathbf{15}_R$-spurions also do not break $SO(2)_S$, the $(\mathbf{6}_L, \mathbf{15}_R)$ does not generate a singlet potential. The $(\mathbf{15}_{AL}, \mathbf{15}_R)$ with $\phi_{15L} = \phi_{15R} = 0$ fulfills all basic conditions, whereas for the $(\mathbf{20}'_L, \mathbf{15}_R)$ we need to choose $\theta_{15R} = 0$, $\phi_{20L} = -\pi/2$. In the latter case, small θ_{20_L}, which is favoured from the Zbb-constraint, leads to a small top mass and comparatively large CPv-inducing term, see Appendix A. Once more, the $S^4(S^6)$ terms arise only at NLO (NNLO) in spurions, while for the $(\mathbf{20}'_L, \mathbf{15}_R)$ interestingly both the Higgs mass and quartic coupling arise at the same order.

We finally move to the $\mathbf{20}'_R$ models, displayed in Table 4, which will turn out to be the most interesting for us. Out of all the models, the one that fits the SNR scenario best is the $(\mathbf{20}'_{AL}, \mathbf{20}'_R)$. Here, while we need a $\mathbf{20}'_{BR}$ contribution to generate the top mass, determined by $y_t \propto y_L y_R^* \sin\theta_{20R1}$, and $\mathbf{20}'_{AR}$ to generate the CPv-inducing operator, an additional $\mathbf{20}'_{CR}$ contribution would not change the order of operators (yet modify their correlation, see below). Accordingly, we initially focus on $\theta_{20L} = 0$, $\theta_{20R2} = 0$, $\phi_{20R1} = \pi/2$, $\phi_{20R2} = 0$.

The same considerations lead to focusing on the $(\mathbf{15}_{AL}, \mathbf{20}'_{ABR})$ setup, while for the $(\mathbf{6}_L, \mathbf{20}'_R)$, both $\mathbf{20}'_{ABR}$ and $\mathbf{20}'_{BCR}$ would work equally fine. Therefore, we display only $\theta_{20R2} = 0$ models in the table. For the Yukawa terms we employ $\phi_{20R1} - \phi_{15L} = \pi$, $\phi_{20R2} - \phi_{15L} = \pi/2$ ($\phi_{20R1} = \pi$, $\phi_{20R2} = -\pi/2$) in the former (latter) case. Note that here, the $\mathbf{6}_L$ and $\mathbf{15}_{AL}$ models predict opposite signs for the h^4 and $h^2 S^2$ terms and thus do not fulfill the conditions for the Z_2 SNR scenario of Section 2.

This can be remedied by allowing nonzero θ_{R2}, where we can fulfill the constraints on signs and magnitude of the couplings for points within $\theta_{20R2} \in (0.70, 1.50) \cup (1.64, 2.45)$ for $\theta_{20R1} \in (1.11, 1.50) \cup (1.11, 1.50) + \pi$ and $\theta_{20R2} \in (0.70, 1.50) + \pi \cup (1.64, 2.45) + \pi$ for $\theta_{20R1} \in (0.70, 1.11) \cup (0.70, 1.11) + \pi$.

Coming back to our model of choice, the $(\mathbf{20}'_{AL}, \mathbf{20}'_{ABR})$, we can easily create the sought pattern of couplings to realize the Z_2 SNR scenario, where the S^6 (S^4) terms arise already at NLO (LO) in spurions, which allows for non-negligible contributions. Also the fact that the Higgs quartic coupling arises at LO in spurions is interesting regarding the naturalness of the setup. We will provide a more quantitative evaluation of this model in the next section.

Table 1. $V(h,S)$ terms obtained via our spurion analysis for t_R a $SO(6)$ singlet. Only leading terms are shown and each entry should be multiplied by $N_c m_*^4/16\pi^2$, while every h or S comes with a factor $1/f$ and every $y_{L,R}$ with a $1/g_*$. The coefficients c_i of the various invariants are just numbered consecutively. Parameters that contribute in the same way in the given approximation were collected into single c_i and we abbreviate $\mathfrak{c}_{2\theta} = \cos 2\theta_{20\mathrm{L}}$, $\mathfrak{s}_\theta^2 = \sin^2\theta_{20\mathrm{L}}$.

		$\mathbf{1}_R$
$\mathbf{6}_L$	h^2	
	h^4	
	h^6	
	S^2	
	S^4	No S-pot
	S^6	
	$h^2 S^2$	
	$h^2 S^4$	
	$h^4 S^2$	
$\mathbf{15}_{\mathrm{A}L}$	h^2	
	h^4	
	h^6	
	S^2	
	S^4	No top mass
	S^6	
	$h^2 S^2$	
	$h^2 S^4$	
	$h^4 S^2$	
$\mathbf{20}'_L$	h^2	$y_L^2\left(\mathfrak{s}_\theta^2 c_1 + \frac{1}{4}\left(4\mathfrak{c}_{2\theta}-3\right)c_2\right)$
	h^4	$-y_L^2\mathfrak{s}_\theta^2\left(c_1 - c_2\right)$
	h^6	$\frac{1}{4}y_L^4\mathfrak{s}_\theta^2\left(-c_4 + 2c_5 + 2c_6 - c_7 - 2\mathfrak{s}_\theta^2\left(4c_3 - 6c_4 + 8c_5 + 6c_6 - 5c_7\right)\right)$
	S^2	$y_L^2\mathfrak{c}_{2\theta}c_2$
	S^4	$\frac{1}{2}y_L^4\mathfrak{c}_{2\theta}^2\left(2c_5 + c_6\right)$
	S^6	$\frac{1}{4}y_L^6\mathfrak{c}_{2\theta}^3 4c_8$
	$h^2 S^2$	$y_L^2\mathfrak{c}_{2\theta}\left(c_1 - c_2\right)$
	$h^2 S^4$	$-\frac{1}{2}y_L^4\mathfrak{c}_{2\theta}^2\left(-2c_4 + 4c_5 + 2c_6 - c_7\right)$
	$h^4 S^2$	$\frac{1}{4}y_L^4\mathfrak{c}_{2\theta}\left(4\mathfrak{s}_\theta^2\left(2c_3 - 4c_4 + 6c_5 + 4c_6 - 3c_7\right) - \left(-c_4 + 2c_5 + 2c_6 - c_7\right)\right)$

Table 2. $V(h,S)$ terms obtained via our spurion analysis for t_R in a $SO(6)$ sextuplet. Only leading terms are shown and each entry should be multiplied by $N_c m_*^4/16\pi^2$, while every h or S comes with a factor $1/f$ and every $y_{L,R}$ with a $1/g_*$. The $\mathbf{15}_L$ model does not generate a CPv-inducing term and is thus displayed in gray. Parameters that contribute in the same way in the given approximation were collected into single c_i and we abbreviate $\mathfrak{c}_{2\theta} = \cos 2\theta_{6\mathrm{R}}$ and $\mathfrak{s}_\theta^2 = \sin^2\theta_{6\mathrm{R}}$ in the first two blocks and $\mathfrak{c}_{2\theta} = \cos 2\theta_{20\mathrm{L}}$ and $\mathfrak{s}_\theta^2 = \sin^2\theta_{20\mathrm{L}}$ in the third, while the other angle is set to zero, respectively.

		$\mathbf{6}_R$
$\mathbf{6}_L$	h^2	$\frac{1}{2}y_L^2 c_1 - y_R^2 \mathfrak{s}_\theta^2 c_2$
	h^4	$\frac{1}{4}y_L^4 c_4 - \frac{1}{2}y_L^2 y_R^2 \mathfrak{s}_\theta^2(-2c_3) + y_R^4 \mathfrak{s}_\theta^4 c_5$
	h^6	$\frac{1}{8}\left(y_L^6 c_8 - 2y_L^4 y_R^2 \mathfrak{s}_\theta^2 c_6 + 4y_L^2 y_R^4 \mathfrak{s}_\theta^4 c_7 - 8y_R^6 \mathfrak{s}_\theta^6 c_9\right)$
	S^2	$y_R^2 \mathfrak{c}_{2\theta} c_2$
	S^4	$y_R^4 \mathfrak{c}_{2\theta}^2 c_5$
	S^6	$y_R^6 \mathfrak{c}_{2\theta}^3 c_9$
	$h^2 S^2$	$\frac{1}{2}y_R^2 \mathfrak{c}_{2\theta}\left(-2y_L^2 c_3 - 4y_R^2 \mathfrak{s}_\theta^2 c_5\right)$
	$h^2 S^4$	$\frac{1}{2}y_R^4 \mathfrak{c}_{2\theta}^2\left(y_L^2 c_7 - 6y_R^2 \mathfrak{s}_\theta^2 c_9\right)$
	$h^4 S^2$	$\frac{1}{4}y_R^2 \mathfrak{c}_{2\theta}\left(y_L^4 c_6 - 4y_L^2 y_R^2 \mathfrak{s}_\theta^2 c_7 + 12y_R^4 \mathfrak{s}_\theta^4 c_9\right)$
$\mathbf{15}_{\mathrm{A}L}$	h^2	$\frac{1}{4}y_L^2 c_1 - y_R^2 \mathfrak{s}_\theta^2 c_2$
	h^4	$\frac{1}{16}y_L^4(c_4 + c_5) - \frac{1}{4}y_L^2 y_R^2 \mathfrak{s}_\theta^2 c_3 + y_R^4 \mathfrak{s}_\theta^4 c_6$
	h^6	$\frac{1}{64}h^6\left(16c_9 y_L^2 y_R^4 \mathfrak{s}_\theta^4 - 4(c_7 + c_8)y_L^4 y_R^2 \mathfrak{s}_\theta^2 + (c_{10} + c_{11} - 8c_{12})y_L^6 - 64c_{13}y_R^6 \mathfrak{s}_\theta^6\right)$
	S^2	$y_L^2 c_1 + y_R^2 \mathfrak{c}_{2\theta} c_2$
	S^4	$y_L^2 y_R^2 \mathfrak{c}_{2\theta} c_3 + \frac{1}{2}y_L^4(2c_4 + c_5) + y_R^4 \mathfrak{c}_{2\theta}^2 c_6$
	S^6	$\frac{1}{2}\left(y_L^4 y_R^2 \mathfrak{c}_{2\theta}(2c_7 + c_8) + y_L^2 y_R^4(\mathfrak{c}_{4\theta} + 1)c_9 + y_L^6(2c_{10} + c_{11}) + 2y_R^6 \mathfrak{c}_{2\theta}^3 c_{13}\right)$
	$h^2 S^2$	$\frac{1}{4}y_L^4(2c_4 + c_5) + \frac{1}{4}y_L^2 y_R^2(3\mathfrak{c}_{2\theta} - 2)c_3 - 2y_R^4 \mathfrak{s}_\theta^2 \mathfrak{c}_{2\theta} c_6$
	$h^2 S^4$	$\frac{1}{8}\left(2y_L^4 y_R^2(2\mathfrak{c}_{2\theta} - 1)(2c_7 + c_8) + 2y_L^2 y_R^4 \mathfrak{c}_{2\theta}(5\mathfrak{c}_{2\theta} - 4)c_9 + 3y_L^6(2c_{10} + c_{11}) - 24y_R^6 \mathfrak{s}_\theta^2 \mathfrak{c}_{2\theta}^2 c_{13}\right)$
	$h^4 S^2$	$\frac{1}{16}\left(y_L^4 y_R^2(c_7(5\mathfrak{c}_{2\theta} - 4)c_7 + (3\mathfrak{c}_{2\theta} - 2)c_8) + 8y_L^2 y_R^4 \mathfrak{s}_\theta^2(1 - 2\mathfrak{c}_{2\theta})c_9 + y_L^6(3c_{10} + 2c_{11}) + 48y_R^6 \mathfrak{s}_\theta^4 \mathfrak{c}_{2\theta} c_{13}\right)$
$\mathbf{20}'_L$	h^2	$y_L^2\left(\mathfrak{s}_\theta^2 c_1 + \frac{1}{4}(4\mathfrak{c}_{2\theta} - 3)c_2\right)$
	h^4	$-y_L^2 \mathfrak{s}_\theta^2(c_1 - c_2)$
	h^6	$\frac{1}{4}\mathfrak{s}_\theta^2 y_L^4\left(-2\mathfrak{s}_\theta^2(4c_6 - 6c_7 + 8c_8 + 6c_9 - 5c_{10}) - (c_7 - 2c_8 - 2c_9 + c_{10})\right)$
	S^2	$y_L^2 \mathfrak{c}_{2\theta} c_2 + y_R^2 c_3$
	S^4	$y_L^2 y_R^2 \mathfrak{c}_{2\theta} c_5 + \frac{1}{2}y_L^4 \mathfrak{c}_{2\theta}^2(2c_8 + c_9) + y_R^4 c_{11}$
	S^6	$\frac{1}{4}\left(y_L^6 \mathfrak{c}_{2\theta}^3 4c_{14} + y_L^4 y_R^2(\mathfrak{c}_{4\theta} + 1)2c_{12} + 4y_L^2 y_R^4 \mathfrak{c}_{2\theta} c_{13} + 4y_R^6 c_{15}\right)$
	$h^2 S^2$	$y_L^2 \mathfrak{c}_{2\theta}(c_1 - c_2)$
	$h^2 S^4$	$\frac{1}{2}y_L^2 \mathfrak{c}_{2\theta}\left(y_L^2 \mathfrak{c}_{2\theta}(2c_7 - 4c_8 - 2c_9 + c_{10}) - 2y_R^2(2c_4 + c_5)\right)$
	$h^4 S^2$	$\frac{1}{4}y_L^4 \mathfrak{c}_{2\theta}\left(4\mathfrak{s}_\theta^2(2c_6 - 4c_7 + 6c_8 + 4c_9 - 3c_{10}) + c_7 - 2c_8 - 2c_9 + c_{10}\right) + y_L^2 y_R^2 \mathfrak{s}_\theta^2(2c_4 + c_5)$

Table 3. $V(h, S)$ terms obtained via our spurion analysis for t_R in a **15** of $SO(6)$. Only leading terms are shown and each entry should be multiplied by $N_c m_*^4/16\pi^2$, while every h or S comes with a factor $1/f$ and every $y_{L,R}$ with a $1/g_*$. Parameters that contribute in the same way in the given approximation were collected into single c_i and we abbreviate $\mathfrak{c}_{2\theta} = \cos 2\theta_{15\,R\,(20L)}$ and $\mathfrak{s}_\theta^2 = \sin^2 \theta_{15\,R\,(20L)}$ in the second (third) block, while the other angle is set to zero, respectively. As discussed in the text, finite values of the angles however do not change the order of terms, here and below.

		$\mathbf{15}_R$
$\mathbf{6}_L$	h^2	
	h^4	
	h^6	
	S^2	
	S^4	No S-potential
	S^6	
	$h^2 S^2$	
	$h^2 S^4$	
	$h^4 S^2$	
$\mathbf{15}_{\mathrm{A}L}$	h^2	$\frac{1}{4} y_L^2 c_1 + \frac{1}{8} y_R^2 (3\mathfrak{c}_{2\theta} - 1) c_2$
	h^4	$\frac{1}{64} \left(2 y_L^2 y_R^2 ((3\mathfrak{c}_{2\theta} - 1) c_3 - 4\mathfrak{s}_\theta^2 c_4) + 4 y_L^4 (c_5 + c_6) + y_R^4 (1 - 3\mathfrak{c}_{2\theta})^2 c_7\right)$
	h^6	$\frac{1}{512} \Big(4 y_L^4 y_R^2 ((3c_8 + 3c_9 + 2c_{12} + 2c_{13}) \mathfrak{c}_{2\theta} - c_8 - c_9 - 2c_{12} - 2c_{13})$ $+ 2 y_L^2 y_R^4 (3\mathfrak{c}_{2\theta} - 1)((3c_{10} + 2c_{11}) \mathfrak{c}_{2\theta} - c_{10} - 2c_{11}) + 8 (c_{14} + c_{15} + c_{16}) y_L^6 + c_{17} y_R^6 (3\mathfrak{c}_{2\theta} - 1)^3\Big)$
	S^2	$y_L^2 c_1$
	S^4	$y_L^4 \frac{1}{2} (2c_5 + c_6)$
	S^6	$\frac{1}{4} y_L^6 (4c_{14} + 2c_{15} + c_{16})$
	$h^2 S^2$	$\frac{1}{32} y_L^2 \left(8 (2c_5 + c_6) y_L^2 + (4c_3 + c_4) y_R^2 (3\mathfrak{c}_{2\theta} - 1)\right)$
	$h^2 S^4$	$\frac{1}{64} y_L^4 \left(12 (4c_{14} + 2c_{15} + c_{16}) y_L^2 + (8c_8 + 4c_9 + 2c_{12} + c_{13}) y_R^2 (3\mathfrak{c}_{2\theta} - 1)\right)$
	$h^4 S^2$	$\frac{1}{256} y_L^2 \Big(y_L^2 y_R^2 ((48c_8 + 24c_9 + 22c_{12} + 14c_{13}) \mathfrak{c}_{2\theta} - 16c_8 - 8c_9 - 18c_{12} - 10c_{13})$ $+ 8 (6c_{14} + 4c_{15} + 3c_{16}) y_L^4 + (4c_{10} + c_{11}) y_R^4 (1 - 3\mathfrak{c}_{2\theta})^2\Big)$
$\mathbf{20'}_L$	h^2	$y_L^2 \left(\mathfrak{s}_\theta^2 c_1 + \frac{1}{4} (4\mathfrak{c}_{2\theta} - 3) c_2\right) + \frac{1}{4} y_R^2 c_3$
	h^4	$-y_L^2 \mathfrak{s}_\theta^2 (c_1 - c_2)$
	h^6	$\frac{1}{4} \mathfrak{s}_\theta^2 \left(y_L^4 \left(-2 (4c_7 - 6c_8 + 8c_9 + 6c_{10} - 5c_{11}) \mathfrak{s}_\theta^2 - c_8 + 2c_9 + 2c_{10} - c_{11}\right) - y_L^2 y_R^2 (c_4 - c_5)\right)$
	S^2	$y_L^2 \mathfrak{c}_{2\theta} c_2$
	S^4	$\frac{1}{2} y_L^4 \mathfrak{c}_{2\theta}^2 (2c_9 + c_{10})$
	S^6	$\frac{1}{4} y_L^6 \mathfrak{c}_{2\theta}^3 4c_{12}$
	$h^2 S^2$	$y_L^2 \mathfrak{c}_{2\theta} (c_1 - c_2)$
	$h^2 S^4$	$\frac{1}{2} y_L^4 \mathfrak{c}_{2\theta}^2 (2c_8 - 4c_9 - 2c_{10} + c_{11})$
	$h^4 S^2$	$\frac{1}{4} \mathfrak{c}_{2\theta} \left(y_L^4 \left(4 (2c_7 - 4c_8 + 6c_9 + 4c_{10} - 3c_{11}) \mathfrak{s}_\theta^2 + c_8 - 2c_9 - 2c_{10} + c_{11}\right) + y_L^2 y_R^2 (c_4 - c_5)\right)$

Table 4. $V(h,S)$ terms obtained via our spurion analysis for t_R in a $\mathbf{20'}_{\mathrm{AB}}$ of $SO(6)$ ($\theta_{20R2} = 0$). This configuration is chosen in order to reproduce a heavy top quark and simultaneously a CPV-inducing term, combining viably with the $\mathbf{20'}_{\mathrm{A}L}$ such as to generate a S^6 term at NLO and fitting our SNR criteria. Only leading terms are shown and each entry should be multiplied by $N_c m_*^4/16\pi^2$, while every h or S comes with a factor $1/f$ and every $y_{L,R}$ with a $1/g_*$. Parameters that contribute in the same way in the given approximation were collected into single c_i and we abbreviate $\mathfrak{c}_{2\theta} = \cos 2\theta_{20\mathrm{R1}}$ and $\mathfrak{s}_\theta^2 = \sin^2\theta_{20\mathrm{R1}}$, while $\theta_{15L}, \theta_{20L} = 0$. The smaller left handed embeddings do not fit the SNR coupling pattern in this choice of angles – for a discussion of nonzero θ_{20R2}, which does allow SNR also here, see main text.

|		$\mathbf{20'}_R$
	h^2	$\frac{1}{2}y_L^2 c_1 + \frac{1}{40}y_R^2\left(11\mathfrak{c}_{2\theta} - 9\right)c_3$
	h^4	$\frac{1}{20}y_R^2\mathfrak{c}_\theta^2\left(c_2 - c_3\right)$
	h^6	$\frac{1}{800}\mathfrak{c}_\theta^2\left(20y_L^2 y_R^2\left(-2c_4\right) + y_R^4\left(11\mathfrak{c}_{2\theta} - 9\right)\left(c_6 - 2c_7\right)\right)$
	S^2	$y_R^2\left(2\mathfrak{s}_\theta^2 c_2 + \frac{1}{5}\left(7\mathfrak{c}_{2\theta} - 3\right)c_3\right)$
$\mathbf{6}_L$	S^4	$y_R^2\frac{1}{5}\left(7\mathfrak{c}_{2\theta} - 3\right)\left(c_2 - c_3\right)$
	S^6	$\frac{4}{25}y_R^4\left(7\mathfrak{c}_{2\theta} - 3\right)\left(c_6 - 2c_7 + \mathfrak{s}_\theta^2\left(5c_5 - 6c_6 + 7c_7\right)\right)$
	$h^2 S^2$	$y_R^2\frac{2}{5}\left(2\mathfrak{c}_{2\theta} - 3\right)\left(c_2 - c_3\right)$
	$h^2 S^4$	$\frac{1}{10}y_L^2 y_R^2\left(7\mathfrak{c}_{2\theta} - 3\right)\left(-2c_4\right)$ $+\frac{1}{200}y_R^4\left(-64\mathfrak{s}_\theta^2\left(25c_5 - 29c_6 + 33c_7\right) + \mathfrak{s}_{2\theta}^2\left(320c_5 - 461c_6 + 602c_7\right) - 56\left(c_6 - 2c_7\right)\right)$
	$h^4 S^2$	$\frac{1}{5}y_L^2 y_R^2\left(2\mathfrak{c}_{2\theta} - 3\right)\left(-2c_4\right) + \frac{1}{200}y_R^4\left(2\mathfrak{s}_\theta^2\left(5c_5 - 28c_6 + 51c_7\right) - 2\left(49\mathfrak{c}_{2\theta} - 51\right)\left(c_6 - 2c_7\right)\right)$
	h^2	$\frac{1}{4}y_L^2 c_1 + \frac{1}{40}y_R^2\left(11\mathfrak{c}_{2\theta} - 9\right)c_3$
	h^4	$\frac{1}{20}y_R^2\mathfrak{c}_\theta^2\left(c_2 - c_3\right)$
	h^6	$\frac{1}{800}y_R^2\mathfrak{c}_\theta^2\left(10y_L^2 c_4 + y_R^2\left(11\mathfrak{c}_{2\theta} - 9\right)\left(c_6 - 2c_7\right)\right)$
	S^2	$y_L^2 c_1 + y_R^2\left(2\mathfrak{s}_\theta^2 c_2 + \frac{1}{5}\left(7\mathfrak{c}_{2\theta} - 3\right)c_3\right)$
$\mathbf{15}_{\mathrm{A}L}$	S^4	$\frac{1}{5}y_R^2\left(7\mathfrak{c}_{2\theta} - 3\right)\left(c_2 - c_3\right)$
	S^6	$\frac{1}{25}y_R^2\left(7\mathfrak{c}_{2\theta} - 3\right)\left(5c_4 y_L^2 + y_R^2\left(2\left(\mathfrak{c}_{2\theta} - 1\right)\left(-5c_5 + 6c_6 - 7c_7\right) + 4\left(c_6 - 2c_7\right)\right)\right)$
	$h^2 S^2$	$\frac{2}{5}y_R^2\left(2\mathfrak{c}_{2\theta} - 3\right)\left(c_2 - c_3\right)$
	$h^2 S^4$	$\frac{1}{200}y_R^2\left(10y_L^2\left(23\mathfrak{c}_{2\theta} - 27\right)c_4\right.$ $\left.+y_R^2\mathfrak{s}_\theta^2\left(-64\left(25c_5 - 29c_6 + 33c_7\right) + \mathfrak{s}_{2\theta}^2\left(320c_5 - 461c_6 + 602c_7\right) - 56\left(c_6 - 2c_7\right)\right)\right)$
	$h^4 S^2$	$\frac{1}{200}y_R^2\left(5y_L^2\left(9\mathfrak{c}_{2\theta} - 11\right)c_4 - y_R^2\left(2\left(49\mathfrak{c}_{2\theta} - 51\right)\left(c_6 - 2c_7\right) - 2\mathfrak{s}_{2\theta}^2\left(5c_5 - 28c_6 + 51c_7\right)\right)\right)$
	h^2	$y_L^2\frac{1}{4}c_2 + \frac{1}{40}y_R^2\left(11\mathfrak{c}_{2\theta} - 9\right)c_4$
	h^4	$\frac{1}{20}y_R^2\mathfrak{c}_\theta^2\left(c_3 - c_4\right)$
	h^6	$\mathfrak{c}_\theta^2\left(\frac{1}{80}y_L^2 y_R^2\left(c_7 - c_8\right) + \frac{1}{800}y_R^4\left(11\mathfrak{c}_{2\theta} - 9\right)\left(c_{17} - 2c_{18}\right)\right)$
	S^2	$y_L^2 c_2 + \frac{1}{5}y_R^2\left(5c_3 - 3c_4 + \mathfrak{c}_{2\theta}\left(-5c_3 + 7c_4\right)\right)$
$\mathbf{20'}_{\mathrm{A}L}$	S^4	$\frac{1}{5}y_R^2\left(7\mathfrak{c}_{2\theta} - 3\right)\left(c_3 - c_4\right)$
	S^6	$\frac{1}{5}y_L^2 y_R^2\left(7\mathfrak{c}_{2\theta} - 3\right)\left(c_7 - c_8\right)$ $-\frac{2}{25}y_R^4\left(7\mathfrak{c}_{2\theta} - 3\right)\left(-5c_{16} + 4c_{17} - 3c_{18} + \mathfrak{c}_{2\theta}\left(5c_{16} - 6c_{17} + 7c_{18}\right)\right)$
	$h^2 S^2$	$y_L^2\left(c_1 - c_2\right) + \frac{2}{5}y_R^2\left(2\mathfrak{c}_{2\theta} - 3\right)\left(c_3 - c_4\right)$
	$h^2 S^4$	$y_L^4\frac{1}{2}\left(2c_{12} - 4c_{13} - 2c_{14} + c_{15}\right)$ $-\frac{1}{20}y_L^2 y_R^2\left(-20c_5 + 12c_6 + 47c_7 - 39c_8 + 44c_9 - 24c_{10} + \mathfrak{c}_{2\theta}\left(20c_5 - 28c_6 - 43c_7 + 51c_8 - 56c_9 + 36c_{10}\right)\right)$ $+\frac{1}{400}y_R^4\left(64\mathfrak{c}_{2\theta}\left(25c_{16} - 29c_{17} + 33c_{18}\right) + \mathfrak{c}_{4\theta}\left(-320c_{16} + 461c_{17} - 602c_{18}\right) - 1280c_{16} + 1283c_{17} - 1286c_{18}\right)$
	$h^4 S^2$	$\frac{1}{4}y_L^4\left(c_{12} - 2c_{13} - 2c_{14} + c_{15}\right)$ $+\frac{1}{40}y_L^2 y_R^2\left(\mathfrak{c}_{2\theta}\left(11c_6 + 9c_7 - 20c_8 + 17c_9 - 17c_{10}\right) - 9c_6 - 11c_7 + 20c_8 - 23c_9 + 23c_{10}\right)$ $+\frac{1}{200}y_R^4\left(-98\mathfrak{c}_{2\theta}\left(c_{17} - 2c_{18}\right) + \mathfrak{c}_{4\theta}\left(-5c_{16} + 28c_{17} - 51c_{18}\right) + 5c_{16} + 74c_{17} - 153c_{18}\right)$
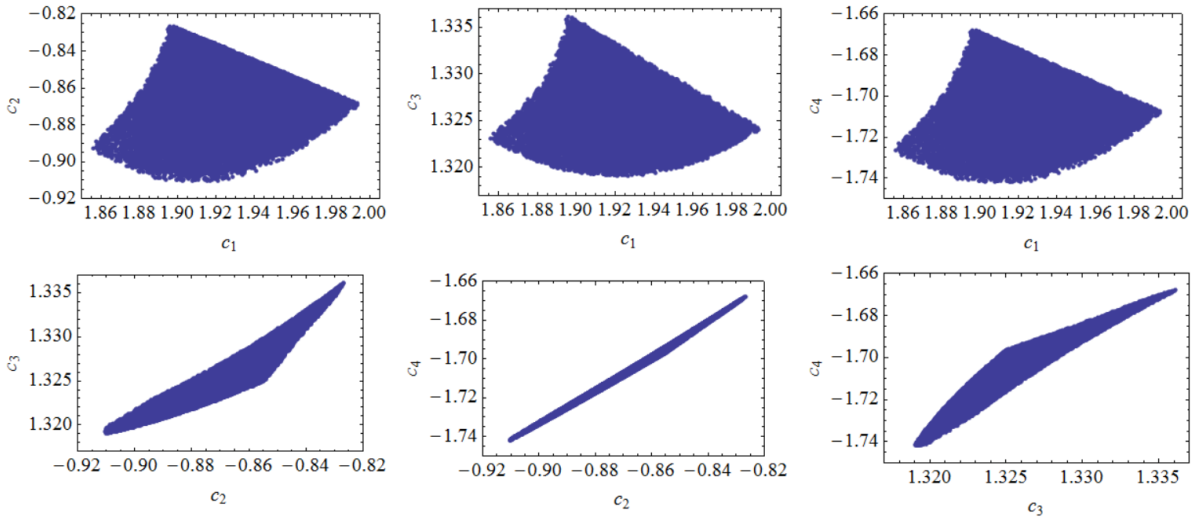
Figure 5. Values of various UV c–parameters that reproduce the IR parameters plotted in Fig. 2. Here, we have chosen $f = 800$ GeV and $g_* = 4$.

4 Matching the EFT to the UV Parameters and Discussion

We now turn to matching the parameters appearing in the potential of Eq. (2.1) to the parameters of the $(\mathbf{20}'_{AL}, \mathbf{20}'_{ABR})$ model, as given in the bottom section of Table 4. For simplicity, we set $y_L = y_R = 1$, but the $y_{L,R}$ dependence can be easily restored through simple rescalings (here, for the $D \leq 4$ operators, $c_{1,2}$ are always multiplied by y_L^2, while $c_{3,4}$ always come with y_R^2).

The coefficients of the dimension–6 operators (h^6, $h^4 S^2$, $h^2 S^4$, and S^6) depend on $\mathcal{O}(10)$ different c–parameters, which means we can treat the cutoff Λ defined in Eq. (2.1) basically as a free parameter, within a *certain range given by the $y_{L,R}/g_*$ scaling*, while the remaining three Wilson coefficients are assumed small enough to not impact our analysis. Setting $\Lambda \sim 1.5$ TeV, see Fig. 1, we now check to which $\mathcal{O}(1)$ coefficient $\bar{c}_4$, appearing in the Lagrangian term $\sim N_c m_*^4/16\pi^2 \, (y_{L,R}/g_*)^4 \, \bar{c}_4 \, S^6/f^6$ (see last block of Table 4), this would correspond. We compare this result to the case of a scaling of $\sim N_c m_*^4/16\pi^2 \, (y_{L,R}/g_*)^6 \, \bar{c}_6 \, S^6/f^6$, holding for all other models considered. Plugging in numerical values of $f = 800$ GeV and $g_* = 4$, we find that $\bar{c}_4 \sim 10$, which is in reasonable agreement with a (sum of) $\mathcal{O}(1)$ number(s), while on the other hand $\bar{c}_6 \sim 200$ would be required. This makes obvious that, while in the latter models the SNR setup is hardly envisagable, it could straightforwardly emerge for the $(\mathbf{20}'_{AL}, \mathbf{20}'_{ABR})$.

The remaining five IR parameters, namely μ_h^2, μ_η^2, $\lambda_h \, \lambda_\eta$, and $\lambda_{h\eta}$, depend on $\mathfrak{c}_\theta$ and four c's, which allows us to express those as functions of the five IR couplings. This exercise gives us an idea of the potential amount of tuning necessary to obtain the potential in Eq. (2.1) from $\mathcal{O}(1)$ c–parameters. We begin by noting that $\mathfrak{c}_\theta$ has

a particularly simple expression, depending (weakly) only on the ratio of the singlet and Higgs quartics:

$$\mathfrak{c}_\theta^2 = \frac{5}{7} \left(1 - \frac{\lambda_\eta}{56\lambda_h} \right)^{-1}. \tag{4.1}$$

Given the small range of λ_η, cf. Fig 2, and the weak dependence of $\mathfrak{c}_\theta$ on λ_η/λ_h, we find a narrow range for the mixing angle, $\mathfrak{c}_\theta \simeq 0.83 - 0.84$. We have checked that this value is safely within the range of values that can successfully generate the baryon asymmetry in the Universe during the EWPhT [3] via the CPv-inducing Yukawa term of (A.8).

As for the remaining four c–parameters, it turns out the values for the IR couplings can be achieved with natural $O(1)$ values of the UV parameters, as illustrated in Fig. 5, which shows viable regions for various combinations of c's. The origin of the apparent strong correlation between c_2, c_3, and c_4 can be straightforwardly traced from the expression of the IR parameters for the the $(\mathbf{20}'_{AL}, \mathbf{20}'_{\mathrm{AB}R})$ model. As $\mathfrak{c}_\theta$ can only vary within a narrow interval, fixing the Higgs quartic and mass squared parameter to their SM values basically determines c_2 and c_3 in terms of c_4 (cf. first two rows of the bottom block of Table 4).

5   Conclusions

We explored a new thermal history in the singlet-extended SM with a spontaneously broken Z_2 symmetry, considering a general scalar potential. Taking into account higher-dimensional terms in the real singlet, that emerge in UV completions of the setup, we found the possibility of non-restoration of the Z_2 symmetry in the early universe. While allowing for a strong first order electroweak phase transition, as required to realize EWBG, the problem of generating domain walls after Z_2 breaking (potentially separating patches with a vanishing total baryon number) is avoided.

After a detailed analysis of this singlet-extended EFT, taking into account various bounds to constrain the parameter space to a well defined viable region, we turned to matching the setup to a motivated UV completion. We found this in the form of a $SO(6)/SO(5)$ nMCHM with a suitable embedding of the SM fermions in the global symmetry. In particular, we provided a comprehensive overview of the scalar potentials generated in all the different possible realizations of the fermion sector, which is also relevant for the question of a viable EWSB (and scalar phenomenology) in nMCHMs in general. Moreover, we provided explicit expressions for the emerging Yukawa couplings in the different models, including CPv terms involving the Higgs and the singlet, that allow to fulfill all Sakarov criteria for a viable baryogenesis.

Finally, identifying the $(\mathbf{20}'_{AL}, \mathbf{20}'_R)$ variant as the most promising model, we presented a numerical analysis and showed that the Z_2 SNR setup emerges with natural values of the model coefficients, matching all criteria identified in the EFT analysis. It would be interesting to explore if the found thermal history could also

emerge in other motivated models beyond the SM, like in the recently proposed model of $SU(6)$ Gauge-Higgs Grand Unification with an extra scalar singlet [36, 37], or in further models with extended scalar sectors.

Acknowledgments

A Yukawa Terms of Different Embeddings

We provide here the explicit results for the Yukawa couplings in the various models considered. For simplicity, we abbreviate the dressed fermion multiplets as $(Q_L'^m)_{ij} = (\Lambda_L'^{m\alpha})_{ij} q_{L\alpha}$, and similar for the right-handed fermions. We obtain

$$
\begin{aligned}
\mathcal{L}_{\text{Yukawa}}^{(6,6)} &= \frac{y_L y_R^*}{g_*} f \left(\bar{Q}_L'^6 \right)_6 \left(t_R'^6 \right)_6 M_1 + \text{h.c.} \\
&= -\frac{y_L y_R^*}{\sqrt{2} g_* f} \bar{t}_L \left[h \sqrt{f^2 - h^2 - S^2} \sin\left(\theta_{6R}\right) + ihS \cos\left(\theta_{6R}\right) \right] M_1 t_R + \text{h.c.}
\end{aligned}
\tag{A.1}
$$

$$
\begin{aligned}
\mathcal{L}_{\text{Yukawa}}^{(15,6)} &= \frac{y_L y_R^*}{g_*} f \left(\bar{Q}_L'^{15} \right)_{6a} \left(t_R'^6 \right)_a M_5 + \text{h.c.} \\
&= -\frac{y_L y_R^*}{2 g_* f} \bar{t}_L h \cos\left(\theta_{6R}\right) M_5 t_R + \text{h.c.}
\end{aligned}
\tag{A.2}
$$

$$
\begin{aligned}
\mathcal{L}_{\text{Yukawa}}^{(20',6)} &= \frac{y_L y_R^*}{g_*} f \left[\left(\bar{Q}_L'^{20'} \right)_{66} \left(t_R'^6 \right)_6 M_1 + \left(\bar{Q}_L'^{20'} \right)_{6a} \left(t_R'^6 \right)_a M_5 \right] + \text{h.c.} \\
&= \frac{y_L y_R^*}{2 g_* f^2} \bar{t}_L \left[-f^2 h \cos\left(\theta_{20L}\right) M_5 + 2hS^2 \cos\left(\theta_{20L}\right) \left(M_1 - M_5 \right) \right. \\
&\qquad \left. + 2ihS \sqrt{f^2 - h^2 - S^2} \sin\left(\theta_{20L}\right) \left(M_1 - M_5 \right) \right] t_R + \text{h.c.}
\end{aligned}
\tag{A.3}
$$

$$
\begin{aligned}
\mathcal{L}_{\text{Yukawa}}^{(15,15)} &= \frac{y_L y_R^*}{g_*} f \left(\bar{Q}_L'^{15} \right)_{6a} \left(t_R'^{15} \right)_{a6} M_5 + \text{h.c.} \\
&= \frac{y_L y_R^*}{4 g_* f} \bar{t}_L \left[\sqrt{2} h \sqrt{f^2 - h^2 - S^2} \sin(\theta_{15R}) + ihS \cos(\theta_{15R}) \right] M_5 t_R + \text{h.c.}
\end{aligned}
\tag{A.4}
$$

$$
\begin{aligned}
\mathcal{L}_{\text{Yukawa}}^{(20',15)} &= \frac{y_L y_R^*}{g_*} f \left(\bar{Q}_L'^{20'} \right)_{6a} \left(t_R'^{15} \right)_{a6} M_5 + \text{h.c.} \\
&= \frac{y_L y_R^*}{4 g_* f} \bar{t}_L \left[h \sqrt{f^2 - h^2 - S^2} \sin\left(\theta_{20L}\right) + ihS \cos\left(\theta_{20L}\right) \right] M_5 t_R + \text{h.c.}
\end{aligned}
\tag{A.5}
$$

$$\mathcal{L}_{\text{Yukawa}}^{(6,20')} = \frac{y_L y_R^*}{g_*} f \left[\left(\bar{Q}_L'^6 \right)_6 \left(t_R'^{20'} \right)_{66} M_1 + \left(\bar{Q}_L'^6 \right)_a \left(t_R'^{20'} \right)_{a6} M_5 \right] + \text{h.c.} \tag{A.6}$$

$$= \frac{y_L y_R^*}{g_* f^2} \bar{t}_L \left[- f^2 h \left\{ \left(\frac{1}{2\sqrt{10}} e^{i\phi_{20R1}} \cos\left(\theta_{20R1}\right) + \sqrt{\frac{3}{5}} \sin\left(\theta_{20R1}\right) \sin\left(\theta_{20R2}\right) \right) M_5 \right. \right.$$

$$\left. - \frac{\sqrt{15}}{6} \sin\left(\theta_{20R1}\right) \sin\left(\theta_{20R2}\right) M_1 \right\}$$

$$+ hS\sqrt{f^2 - h^2 - S^2} e^{i\phi_{20R2}} \cos\left(\theta_{20R2}\right) \sin\left(\theta_{20R1}\right) \left(M_5 - M_1\right)$$

$$+ \frac{hS^2 \left(\sqrt{2} e^{i\phi_{20R1}} \cos\left(\theta_{20R1}\right) - \sqrt{3} \sin\left(\theta_{20R1}\right) \sin\left(\theta_{20R2}\right) \right)}{\sqrt{5}} \left(M_5 - M_1\right)$$

$$\left. - \frac{h^3 \left(\sqrt{2} e^{i\phi_{20R1}} \cos\left(\theta_{20R1}\right) + 4\sqrt{3} \sin\left(\theta_{20R1}\right) \sin\left(\theta_{20R2}\right) \right)}{4\sqrt{5}} \left(M_5 - M_1\right) \right] t_R$$

$$+ \text{h.c.}$$

$$\overset{here}{=} - \frac{y_L y_R^*}{g_* f^2} \bar{t}_L \left[f^2 h \frac{\cos\left(\theta_{20R1}\right)}{2\sqrt{10}} M_5 + i \cdot hS\sqrt{f^2 - h^2 - S^2} \sin\left(\theta_{20R1}\right) \left(M_5 - M_1\right) \right.$$

$$\left. + \left(\sqrt{\frac{2}{5}} hS^3 - \frac{1}{2\sqrt{10}} h^3 \right) \cos\left(\theta_{20R1}\right) \left(M_5 - M_1\right) \right] + \text{h.c.}$$

$$\mathcal{L}_{\text{Yukawa}}^{(15,20')} = \frac{y_L y_R^*}{g_*} f \left(\bar{Q}_L'^{15'} \right)_{6a} \left(t_R'^{20'} \right)_{a6} M_5 + \text{h.c.}$$

$$= i \frac{y_L y_R^*}{4 g_* f} \bar{t}_L e^{-i\phi_{15L}} \left[\sqrt{2} h e^{i\phi_{20R2}} \sin\left(\theta_{20R1}\right) \cos\left(\theta_{20R2}\right) \sqrt{f^2 - h^2 - S^2} \right. \tag{A.7}$$

$$\left. + \sqrt{5} h S e^{i\phi_{20R1}} \cos\left(\theta_{20R1}\right) \right] M_5 t_R + \text{h.c.}$$

$$\overset{here}{=} - \frac{y_L y_R^*}{4 g_* f} \bar{t}_L \left[\sqrt{2} \sin\left(\theta_{20R1}\right) \cdot h\sqrt{f^2 - h^2 - S^2} + i\sqrt{5} \cdot hS \cos\left(\theta_{20R1}\right) \right] t_R M_5 + \text{h.c.}$$

$$\mathcal{L}_{\text{Yukawa}}^{(20',20')} = \frac{y_L y_R^*}{g_*} f \left[\left(\bar{Q}_L'^{20'} \right)_{66} \left(t_R'^{20'} \right)_{66} M_1 + \left(\bar{Q}_L'^{20'} \right)_{6a} \left(t_R'^{20'} \right)_{a6} M_5 \right] + \text{h.c.} \tag{A.8}$$

$$= \frac{y_L y_R^*}{g_* f^3} \bar{t}_L \left[- f^2 h \sqrt{f^2 - h^2 - S^2} \frac{\sin\left(\theta_{20R1}\right) M_5}{2\sqrt{2}} - i f^2 hS \frac{3 \cos\left(\theta_{20R1}\right) M_5}{4\sqrt{5}} \right.$$

$$- hS^2 \sqrt{f^2 - h^2 - S^2} \sqrt{2} \sin\left(\theta_{20R1}\right) \left(M_1 - M_5\right)$$

$$\left. + \frac{i}{2\sqrt{5}} \left(h^3 S - 4 hS^3 \right) \cos\left(\theta_{20R1}\right) \left(M_1 - M_5\right) \right] t_R + \text{h.c.} \, ,$$

where M_1, M_5 are the form factors associated to invariants from $SO(5)$ singlets and fiveplets. These expressions allow to explicitly see the generation of the top mass as well as to estimate the size of CPv induced in terms of the mixing angles.

References

[1] A. D. Sakharov. Violation of CP Invariance, C asymmetry, and baryon asymmetry of the universe. *Pisma Zh. Eksp. Teor. Fiz.*, 5:32–35, 1967.

[2] Ben Gripaios, Alex Pomarol, Francesco Riva, and Javi Serra. Beyond the Minimal Composite Higgs Model. *JHEP*, 04:070, 2009, 0902.1483.

[3] Jose R. Espinosa, Ben Gripaios, Thomas Konstandin, and Francesco Riva. Electroweak Baryogenesis in Non-minimal Composite Higgs Models. *JCAP*, 01:012, 2012, 1110.2876.

[4] J. R. Espinosa and M. Quiros. The Electroweak phase transition with a singlet. *Phys. Lett. B*, 305:98–105, 1993, hep-ph/9301285.

[5] Jose Ramon Espinosa and Mariano Quiros. Novel Effects in Electroweak Breaking from a Hidden Sector. *Phys. Rev. D*, 76:076004, 2007, hep-ph/0701145.

[6] Stefano Profumo, Michael J. Ramsey-Musolf, and Gabe Shaughnessy. Singlet Higgs phenomenology and the electroweak phase transition. *JHEP*, 08:010, 2007, 0705.2425.

[7] Jose R. Espinosa, Thomas Konstandin, and Francesco Riva. Strong Electroweak Phase Transitions in the Standard Model with a Singlet. *Nucl. Phys. B*, 854:592–630, 2012, 1107.5441.

[8] Vernon Barger, Daniel J. H. Chung, Andrew J. Long, and Lian-Tao Wang. Strongly First Order Phase Transitions Near an Enhanced Discrete Symmetry Point. *Phys. Lett. B*, 710:1–7, 2012, 1112.5460.

[9] James M. Cline and Kimmo Kainulainen. Electroweak baryogenesis and dark matter from a singlet Higgs. *JCAP*, 01:012, 2013, 1210.4196.

[10] David Curtin, Patrick Meade, and Chiu-Tien Yu. Testing Electroweak Baryogenesis with Future Colliders. *JHEP*, 11:127, 2014, 1409.0005.

[11] Gowri Kurup and Maxim Perelstein. Dynamics of Electroweak Phase Transition In Singlet-Scalar Extension of the Standard Model. *Phys. Rev. D*, 96(1):015036, 2017, 1704.03381.

[12] Marcela Carena, Zhen Liu, and Marc Riembau. Probing the electroweak phase transition via enhanced di-Higgs boson production. *Phys. Rev. D*, 97(9):095032, 2018, 1801.00794.

[13] Marcela Carena, Zhen Liu, and Yikun Wang. Electroweak phase transition with spontaneous Z_2-breaking. *JHEP*, 08:107, 2020, 1911.10206.

[14] Ya. B. Zeldovich, I. Yu. Kobzarev, and L. B. Okun. Cosmological Consequences of the Spontaneous Breakdown of Discrete Symmetry. *Zh. Eksp. Teor. Fiz.*, 67:3–11, 1974.

[15] James M. Cline, Avi Friedlander, Dong-Ming He, Kimmo Kainulainen, Benoit Laurent, and David Tucker-Smith. Baryogenesis and gravity waves from a

UV-completed electroweak phase transition. *Phys. Rev. D*, 103(12):123529, 2021, 2102.12490.

[16] Ville Vaskonen. Electroweak baryogenesis and gravitational waves from a real scalar singlet. *Phys. Rev. D*, 95(12):123515, 2017, 1611.02073.

[17] Albert M Sirunyan et al. Search for invisible decays of a Higgs boson produced through vector boson fusion in proton-proton collisions at $\sqrt{s} = 13$ TeV. *Phys. Lett. B*, 793:520–551, 2019, 1809.05937.

[18] Morad Aaboud et al. Combination of searches for invisible Higgs boson decays with the ATLAS experiment. *Phys. Rev. Lett.*, 122(23):231801, 2019, 1904.05105.

[19] Stefania De Curtis, Luigi Delle Rose, and Giuliano Panico. Composite Dynamics in the Early Universe. *JHEP*, 12:149, 2019, 1909.07894.

[20] David B. Kaplan. Flavor at SSC energies: A New mechanism for dynamically generated fermion masses. *Nucl. Phys.*, B365:259–278, 1991.

[21] Kaustubh Agashe, Roberto Contino, and Alex Pomarol. The Minimal composite Higgs model. *Nucl. Phys.*, B719:165–187, 2005, hep-ph/0412089.

[22] Roberto Contino, Yasunori Nomura, and Alex Pomarol. Higgs as a holographic pseudoGoldstone boson. *Nucl. Phys.*, B671:148–174, 2003, hep-ph/0306259.

[23] Roberto Contino, Leandro Da Rold, and Alex Pomarol. Light custodians in natural composite Higgs models. *Phys. Rev.*, D75:055014, 2007, hep-ph/0612048.

[24] Mikael Chala, Gauthier Durieux, Christophe Grojean, Leonardo de Lima, and Oleksii Matsedonskyi. Minimally extended SILH. *JHEP*, 06:088, 2017, 1703.10624.

[25] Ligong Bian, Yongcheng Wu, and Ke-Pan Xie. Electroweak phase transition with composite Higgs models: calculability, gravitational waves and collider searches. *JHEP*, 12:028, 2019, 1909.02014.

[26] Ke-Pan Xie, Ligong Bian, and Yongcheng Wu. Electroweak baryogenesis and gravitational waves in a composite Higgs model with high dimensional fermion representations. *JHEP*, 12:047, 2020, 2005.13552.

[27] Michele Redi and Andrea Tesi. Implications of a Light Higgs in Composite Models. *JHEP*, 10:166, 2012, 1205.0232.

[28] Christoph Niehoff, Peter Stangl, and David M. Straub. Electroweak symmetry breaking and collider signatures in the next-to-minimal composite Higgs model. *JHEP*, 04:117, 2017, 1611.09356.

[29] Giuliano Panico and Andrea Wulzer. *The Composite Nambu-Goldstone Higgs*, volume 913. Springer, 2016, 1506.01961.

[30] Sidney R. Coleman, J. Wess, and Bruno Zumino. Structure of phenomenological Lagrangians. 1. *Phys. Rev.*, 177:2239–2247, 1969.

[31] Curtis G. Callan, Jr., Sidney R. Coleman, J. Wess, and Bruno Zumino. Structure of phenomenological Lagrangians. 2. *Phys. Rev.*, 177:2247–2250, 1969.

[32] G. F. Giudice, C. Grojean, A. Pomarol, and R. Rattazzi. The Strongly-Interacting Light Higgs. *JHEP*, 06:045, 2007, hep-ph/0703164.

[33] Giuliano Panico, Michele Redi, Andrea Tesi, and Andrea Wulzer. On the Tuning and the Mass of the Composite Higgs. *JHEP*, 03:051, 2013, 1210.7114.

[34] Oleksii Matsedonskyi, Giuliano Panico, and Andrea Wulzer. Light Top Partners for a Light Composite Higgs. *JHEP*, 01:164, 2013, 1204.6333.

[35] Adrian Carmona and Florian Goertz. A naturally light Higgs without light Top Partners. *JHEP*, 05:002, 2015, 1410.8555.

[36] Andrei Angelescu, Andreas Bally, Simone Blasi, and Florian Goertz. Minimal SU(6) Gauge-Higgs Grand Unification. 4 2021, 2104.07366.

[37] Andrei Angelescu, Andreas Bally, Simone Blasi, and Florian Goertz. Unification of Gauge Symmetries... including their breaking. In *European Physical Society Conference on High Energy Physics 2021*, 9 2021, 2109.14538.